

Reanalysis-driven climate simulation over CORDEX North America domain using the Canadian Regional Climate Model, version 5: model performance evaluation

A. Martynov · R. Laprise · L. Sushama ·
K. Winger · L. Šeparović · B. Dugas

Received: 30 July 2012 / Accepted: 18 April 2013 / Published online: 7 May 2013
© The Author(s) 2013. This article is published with open access at Springerlink.com

Abstract The performance of reanalysis-driven Canadian Regional Climate Model, version 5 (CRCM5) in reproducing the present climate over the North American COordinated Regional climate Downscaling EXperiment domain for the 1989–2008 period has been assessed in comparison with several observation-based datasets. The model reproduces satisfactorily the near-surface temperature and precipitation characteristics over most part of North America. Coastal and mountainous zones remain problematic: a cold bias (2–6 °C) prevails over Rocky Mountains in summertime and all year-round over Mexico; winter precipitation in mountainous coastal regions is overestimated. The precipitation patterns related to the North American Monsoon are well reproduced, except on its northern limit. The spatial and temporal structure of the Great Plains Low-Level Jet is well reproduced by the model; however, the night-time precipitation maximum in the jet area is underestimated. The performance of CRCM5 was assessed against earlier CRCM versions and other RCMs. CRCM5 is shown to have been substantially improved compared to CRCM3 and CRCM4 in terms of seasonal mean statistics, and to be comparable to other modern RCMs.

Keywords CRCM5 · CORDEX · Regional climate modelling · North American Monsoon · Great Plains Low-Level Jet · Precipitation cycle · Dynamical downscaling

1 Introduction

The Canadian Regional Climate Model, version 5 (CRCM5) is contributing to the COordinated Regional climate Downscaling EXperiment (CORDEX) program (Giorgi et al. 2009; http://wcrp.ipsl.jussieu.fr/SF_RCD_CORDEX.html; <http://www.meteo.unican.es/en/projects/CORDEX>). Within the CORDEX framework, climate projections made with several Global Climate Models (GCMs) for the Coupled Model Intercomparison Project Phase 5 (CMIP5) are dynamically downscaled by Regional Climate Models (RCMs) over selected continent-scale regional domains. According to the CORDEX project requirements, the performance of participating RCMs in reproducing the recent and present climate has to be assessed, over respective domains, by comparing ERA-Interim driven simulations to available observations.

CRCM5's contribution to CORDEX includes simulations over two CORDEX domains—North America and Africa. The present article describes the performance of CRCM5 in an ERA-Interim reanalysis-driven simulation for the 1989–2008 period over the North American domain. The results corresponding to the future climate simulation over North America are being presented in a companion article by Šeparović et al. (2013). Current and future climate simulations over Africa are presented in Hernández-Díaz et al. (2012) and Laprise et al. (2013), respectively.

A. Martynov · R. Laprise · L. Sushama · K. Winger ·
L. Šeparović · B. Dugas
Centre ESCER (Étude et la Simulation du Climat à l'Échelle
Régionale), Département des sciences de la Terre et de
l'atmosphère, Université du Québec à Montréal,
Montreal, QC, Canada

A. Martynov (✉)
Oeschger Centre for Climate Change Research,
Institute of Geography, University of Bern, Bern, Switzerland
e-mail: andrey.martynov@giub.unibe.ch

The CORDEX framework provides an opportunity to further assess the skill of RCMs over several regions, including North America. Previous evaluations of RCM simulations of the recent climate over the whole North American continent have been realized within Model Intercomparison Projects (MIPs) such as the Project to Intercompare Regional Climate Simulations (PIRCS) (Gutowski et al. 1998; Takle et al. 1999; Anderson et al. 2003) and North American Regional Climate Change Assessment Program (NARCCAP) (Mearns et al. 2009, 2012; Gutowski et al. 2010).

Gutowski et al. (2010) studied the performance of six GCM-driven RCMs in simulating the extreme monthly precipitations over North America for the 1981–1999 period within the NARCCAP project. Two climatologically homogenous regions were analyzed in detail. It was shown that both individually and collectively the RCMs were able to reproduce correctly the precipitation patterns and monthly precipitation extreme statistics over Coastal California, while less convincing results were obtained for the Upper Mississippi region.

Recently the performance of six reanalysis-driven RCMs, participating in the first phase of the NARCCAP project, has been thoroughly examined by Mearns et al. (2012). Extensive analysis of continental-scale and subdomain-focused 2-m air temperature and precipitation fields, simulated by participating models, in comparison with a set of observation-based datasets, showed the relative strong and weak points of participating models. The article also highlighted difficulties in comparing models with observations and between different models.

Different versions of the Canadian Regional Climate Model (CRCM) have been used for simulating the climate of North America, and their performance—both over the whole simulation domains and over subregions—has been evaluated. For the 3rd generation of the model such work has been performed among others by Jiao and Caya (2006), and for 4th generation by Music and Caya (2007), Brochu and Laprise (2007), de Elía and Côté (2010), and Mladjic et al. (2011). The most recent, 5th generation, CRCM5 has recently been applied over the African CORDEX domain by Hernández-Díaz et al. (2012). It is important to mention that the CRCM5 model is an entirely new model, not directly based on earlier CRCM versions 3 and 4. While some features, such as the use of semi-Lagrangian transport, are common in all CRCM versions CRCM5 employs subgrid-scale physical packages that are different from those used in CRCM3 and CRCM4; hence CRCM5 should in all practical aspects be considered as a separate RCM, independent from earlier CRCM versions.

The quality of CRCM5 climate simulations over North America will here be assessed primarily by comparing simulated time- and area-averaged values of important

climate variables, such as near-surface air temperature and precipitation, with available observation datasets, over the whole continent and its homogenous subregions. It is also important to note that the skill of climate models depends on how they reproduce the key elements of the climate system, including major atmospheric circulation patterns and more local mesoscale and synoptic phenomena. For this reason the skill of CRCM5 in reproducing two important elements of the climate system of North America, the North American Monsoon (NAM) and the Great Plains Low-Level Jet (GPLLJ), is also analysed in the present article.

The NAM strongly influences the climate of the Southwestern part of the North American continent in warm season (e.g., Stensrud et al. 1995). Caused primarily by strong annual variations of the temperature contrast between land and ocean, NAM brings important increases in rainfall in July–September over northwestern Mexico and southwestern United States (extending northwards to Arizona, New Mexico and Colorado). During the life cycle of the NAM, the subtropical east Pacific ridge moves northward during the summer months, with moisture transported northwards from the Gulf of California and the eastern Pacific deep inland by the Gulf of California Low-Level Jet (GCLLJ). In the presence of sufficient amount of precipitable water, deep monsoonal convection is developed over mountainous regions along the West Coast, bringing along precipitation in various forms, including violent thunderstorms. The monsoon matures in July–August, reaching the northern limit of its evolution, and then retreats in September–October.

Previous studies have assessed the North American Monsoon System (NAMS) as simulated by GCMs (Chakraborty and Krishnamurti 2003; Collier and Zhang 2006) and RCMs (Saleeby and Cotton 2004; Cerezo-Mota et al. 2011). The NAM has been studied extensively within the North American Monsoon Experiment (NAME) (Higgins and Gochis 2007). The NAME Model Assessment Project (NAMAP) focussed on simulations of selected summer periods by numerous GCMs and RCMs. The first stage of the project was centred on the 1990 warm season (Gutzler et al. 2005), and the second stage (NAMAP2), on the 2004 warm season when an extensive field campaign was performed. Six GCMs and four RCMs participated in NAMAP2 (Gutzler et al. 2009); it has been shown that GCMs do not have sufficient horizontal resolution to correctly reproduce the complex structure of atmospheric circulation associated with NAM. In our assessment of the CRCM5 performance in simulating NAM, we will investigate the characteristics of precipitation over the subregions proposed by Gutzler et al. (2009).

The GPLLJ has also been a topic of extensive studies. The importance of GPLLJ for the North American climate

has been underlined by numerous authors, for example Stensrud (1996), Higgins et al. (1997). The GPLLJ is a relatively narrow band of strong southern winds in the lower troposphere (800–1,000 hPa) that is formed over central USA along the eastern slope of the Rocky Mountains in summertime (July–August). It is associated with strong advection of the moisture from the Gulf of Mexico deep into the continent and, consequently, with enhanced precipitation and thunderstorm activity during the summer season. The diurnal cycle of GPLLJ—related precipitation is noticeably different from usual afternoon precipitation peak, typical for inland mid-latitude regions. Instead, in the GPLLJ zone, the deep convection reaches its maximum between midnight and early morning, as is more typical of tropical climate. Two basic theories were proposed for describing the peculiarities of GPLLJ: the inertial oscillation, initiated by stabilization of the planetary boundary layer at sunset (Blackadar 1957) and the diurnal buoyancy-driven flow over the Rocky Mountains slope (Holton 1967). It was shown by Jiang et al. (2007) that both mechanisms are important for the formation of GPLLJ and neither of them can be neglected.

Numerous studies of the GPLLJ region using simulations by GCMs (Jiang et al. 2007; Cook et al. 2008) and RCM and high-resolution regional reanalyses (Rife et al. 2010; Wang et al. 2010; Cerezo-Mota et al. 2011) have been performed. While the detailed study of GPLLJ is not the main objective of the present study, we will use the approaches developed in these studies for the general evaluation of the CRCM5 performance in reproducing the GPLLJ. The spatial structure and diurnal cycle of simulated GPLLJ and associated precipitation will be examined and compared with reanalysis and observation data.

The article is organized as follows. The CRCM5 model and configuration of simulation are described in Sect. 2. In Sect. 3, the general performance of the simulation is assessed at the North American continental scale. In Sect. 4, the performance of the model over geographically and climatologically homogenous subdomains of the continent is analyzed. The comparison of CRCM5 simulations with observation-based climatology and with earlier CRCM versions and other RCMs is presented in Sect. 5. In Sects. 6 and 7 the ability of CRCM5 to reproduce adequately the NAMS and GPLLJ is evaluated, respectively. Summary and conclusions are presented in Sect. 8.

2 Tools and methods

2.1 Regional Climate Model description

The fifth-generation of the Canadian Regional Climate Model (CRCM5), developed at the *Centre pour l'Étude et*

la Simulation du Climat à l'Échelle Régionale (ESCCER Centre) at the Université du Québec à Montréal (UQAM), is based on a limited-area version of the Global Environment Multiscale (GEM) model used for Numerical Weather Prediction at Environment Canada (Côté et al. 1998). GEM employs semi-Lagrangian transport and (quasi) fully implicit marching scheme. In its fully elastic non-hydrostatic formulation (Yeh et al. 2002), GEM uses a vertical coordinate based on hydrostatic pressure (Laprise 1992). The detailed description of the CRCM5 model can be found in Zadra et al. (2008), Martynov et al. (2012), Hernández-Díaz et al. (2012). The following physical parameterizations, inherited from GEM, are used in CRCM5: deep convection following Kain and Fritsch (1990), shallow convection based on a transient version of Kuo (1965) scheme (Bélair et al. 2005), large-scale condensation (Sundqvist et al. 1989), correlated-K solar and terrestrial radiations (Li and Barker 2005), and subgrid-scale orographic gravity-wave drag (McFarlane 1987). The low-level orographic blocking parameterization of Zadra et al. (2003), with recent modifications described in Zadra et al. (2012) is also used. The planetary boundary layer parameterization (Benoît et al. 1989; Delage and Girard 1992; Delage 1997) has also been modified as described in Zadra et al. (2012), introducing turbulent hysteresis, i.e. an asymmetric TKE evolution near the critical Richardson number by transition between turbulent and laminar regimes.

Some important modifications were introduced to the physical parameterization of the model in order to improve its performance for regional climate. This includes a change to the planetary boundary layer parameterization consisting of reducing turbulent vertical fluxes under very stable conditions: vertical mixing is suppressed at Richardson number values $R_i > 7/60 \approx 0.12$. The interactively coupled one-dimensional lake model FLake (Mironov et al. 2010) has been introduced into the CRCM5 and the performance of the lake-coupled model has been evaluated by Martynov et al. (2012). Interactively coupled FLake model is applied both to resolved and subgrid lakes, following the mosaic approach. The Canadian land-surface scheme CLASS (Verseghy 1991, 2009) version 3.5, allowing for a mosaic representation of land-surface types and a flexible number of layers and depth, has been implemented in CRCM5 with some modifications. The ECOCLIMAP formula for bare soil albedo (Masson et al. 2003) is used instead of the default values in CLASS. The snow thermal conductivity is calculated following Sturm et al. (1997).

2.2 Domain settings and simulation configuration

A 50-year-long simulation (1959–2008) has been performed over the North American continent and

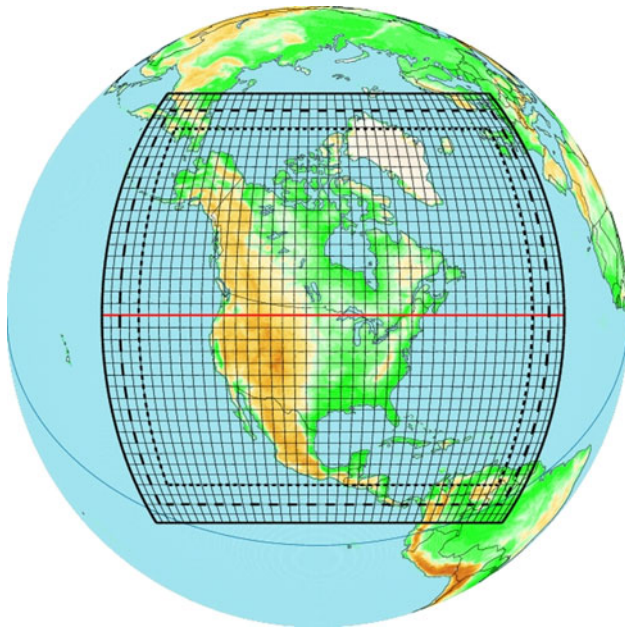


Fig. 1 The simulation grid: rotated lat-lon 212×200 points grid on 0.44° horizontal grid mesh (only every 5th grid point is displayed). The limits of the external ‘halo’ and the Davies sponge zones (each 10 grid point wide) are indicated by the *dashed* and *dotted* lines, respectively. The remaining free innermost domain consists of 172×160 grid points. The grid equator is shown in *red*

neighbouring oceans and islands. The rotated latitude-longitude grid with spacing of 0.44° and of the total size of 212×200 grid points was implemented, as shown in Fig. 1; this domain exceeds the minimum domain size requested by CORDEX. The outer twenty grid points around the perimeter of the domain are used for nesting: the outermost 10 grid points serve as reanalysis-driven “halo” for providing upstream data in the semi-Lagrangian interpolation, and the next 10 grid-point band serves as Davies sponge where CRCM5 atmospheric variables are damped towards the driving fields. This leaves a free inner domain of 172×160 grid points. During the initial period of simulation, 1959–1988, CRCM5 was driven by ERA40 reanalysis and during the period 1989–2008 by the ERA-Interim reanalysis. Lateral boundary conditions on pressure levels were used for driving the regional model: air temperature, horizontal wind components, specific humidity and mean sea level pressure. The sea surface temperature (SST) and sea ice fraction were externally prescribed: during the initial period (1959–1988) AMIP II monthly data (Kanamitsu et al. 2002) were used and for the rest of simulation, ERA-Interim six-hourly data were implemented. Following the CORDEX simulation design specifications, the optional large-scale spectral nudging was turned off in this simulation. The simulation was performed with 20-min timestep, 56 terrain-following levels in

atmosphere with the top level near 10 hPa and the lowest level at $0.996 \times$ surface pressure.

In CLASS, 26 soil layers were used, reaching the maximum depth of 60 m. The ECOCLIMAP geophysical fields for sand and clay (Masson et al. 2003) have been implemented. Otherwise, United States Geology Survey (USGS) geophysical fields were used in the simulation. In order to better reproduce the real vegetation, the fields representing the distribution and characteristics of vegetation have been slightly modified based on comparison with other vegetation/land usage databases and with high-resolution satellite images. Fifty percent of the bare soil fraction has been filled with surrounding vegetation or short grass and forbs. In the boreal forest and north of it, 30 % of bare soil was added to the following vegetation types: needleleaves, deciduous broadleaves, deciduous shrubs, mixed wood forests. Thirty percent of “crops” have been converted to “short grass and forbs”. Although no organic soils were used in the simulation, peatlands were introduced as a separate surface type.

The realistic worldwide lake depth database (Kourzeva 2010) has been used, with the maximum lake depth limitation of 60 m as required by the FLake model. In the absence of reliable data on the shortwave radiation extinction coefficient for the majority of lakes, a constant value of 0.2 m^{-1} is used.

3 Continent-scale performance

The general ability of the model to reproduce the climate over a 20-year-long simulation (1989–2008) is assessed by comparing simulated climate fields with ERA-Interim reanalysis and different observation databases. The list of reference datasets, used in the article, is shown in Table 1.

In Fig. 2 comparison of seasonal multi-annually averaged sea-level atmospheric pressure (MSLP) between CRCM5 and ERA-Interim is presented. In Fig. 2c the difference of mean sea level pressure between CRCM5 and ERA-Interim is shown. Over most part of the domain the difference is small, within ± 2 hPa. The differences are largest in summer over the Southern Rocky Mountains region, where the sea level pressure in CRCM5 is lower than that in ERA-Interim by 5–7 hPa, and in winter over Greenland, where the CRCM5 pressure is 5–6 hPa higher than that of ERA-Interim. The MSLP bias seems closely related to T2m bias, with low/high pressure bias where there is warm/cold bias, supporting the hypothesis that the MSLP bias result in part from the reduction to sea level below high topography.

In Fig. 3 the comparison of 2-m air temperature is shown between CRCM5 simulation data, ERA-Interim reanalysis, CRU TS3.1 and UDel datasets. In summertime

Table 1 Boundary forcing and reference datasets; names, types, data use periods, data frequency, grid mesh parameters, reference variables used in the study, reference publications (if available) and data sources are indicated

Name, data type and use	Data use period and data frequency	Grid mesh	Reference variables	Reference publication and data source
ERA-40	1959–1988	Global $2.5^\circ \times 2.5^\circ$		Uppala et al. (2005)
Reanalysis boundary forcing	6-hourly			ECMWF web site: http://www.ecmwf.int/research/era/do/get/era-40
ERA-Interim reanalysis boundary forcing and reference	1989–2008 6-hourly	Global $2^\circ \times 2^\circ$ (forcing) $1.5^\circ \times 1.5^\circ$ (reference)	2 m air temperature Surface and sea level pressure Wind components	Dee et al. (2011) ECMWF web site: http://www.ecmwf.int/research/era/do/get/era-interim
CRU TS3.10	1989–2008 Monthly	$0.5^\circ \times 0.5^\circ$ Global	2 m air temperature Precipitation rate	Mitchell and Jones (2005) Centre for Environmental Data Archival web site: http://badc.nerc.ac.uk/data/cru
GPCP-1dd	1998–2008 Daily	$1^\circ \times 1^\circ$ Global	Precipitation rate	Huffman et al. (2001)
Observation-based reference				NASA web site: http://precip.gsfc.nasa.gov/gpcp_daily_comb.html
TRMM	1998–2008, 2001–2008 3-hourly	$0.25^\circ \times 0.25^\circ$ (50°S – 50°N)	Precipitation rate	NASA web site: http://trmm.gsfc.nasa.gov/
Observation-based reference				
UDEL (Willmott and Matsuura)	1989–2008 Monthly	$0.5^\circ \times 0.5^\circ$ global	2 m air temperature Precipitation rate	Willmott and Matsuura (1995) NOAA/OAR/ESRL PSD, Boulder, Colorado, USA web site: http://www.esrl.noaa.gov/psdl/
Observation-based reference				

(JJA) the difference between CRCM5 simulations and observations and reanalysis is very small or weakly positive over most part of the region; there are however substantial cold biases over Mexico, Florida, Alaska, the north of Québec and the Canadian Archipelago. It should be noted that there are important differences between ERA-Interim reanalysis, CRU TS3.1 and UDEL observation datasets, especially over the northern part of the continent where observations are scarcely available. The difference of temperatures over oceans is only presented for ERA-Interim, because CRU TS3.1 and UDEL data are not available over oceans. Over most part of the oceans within the simulation domain there is no important bias between CRCM5 simulation and ERA-Interim data, owing to the fact that the ERA-Interim SST was used in the simulation. A small negative bias of up to -2°C can be noted over the Arctic Ocean; it becomes stronger in the vicinity of the Canadian Arctic Archipelago, where comparable bias is present over the land surface. We note that the aforementioned large difference of mean sea level pressure over Greenland (Fig. 2) results from the temperature differences shown in Fig. 3.

In wintertime (DJF) there is an extensive region of cold bias over the southwestern part of the continent, including Mexico, the Rocky Mountains region, the Great Plains and Prairies and the Deep South; a cold bias remains over inner Alaska, Baffin Island, northern Québec and Newfoundland and Labrador coastal zones. In the zone of boreal forests, tundra and to some extent in the northern part of Rocky Mountains, weak or positive bias is noted. In the region of Sawatch Range, Colorado, little bias or a slightly positive bias is present, as opposed to the negative bias in surrounding mountainous area, which appears to be related in part to the specified vegetation distribution (not shown). As in summer, there is substantial difference between three reference datasets, especially over the northern part of the continent and over Greenland, where observations are scarce and hence reanalysis data and observation datasets can be biased. Due to the discrepancies between reference datasets, only the strongest and most generalized biases of CRCM5 can be ascertained.

Small biases in 2-m air temperature are noted over open oceans where SST are prescribed from reanalyses. But when sea ice is present in the reanalyses, CRCM5 computes the ice surface temperature by solving a heat balance equation. The larger surface air temperature bias over the Hudson Bay and Canadian Archipelago in winter is indicative of the fact that CRCM5 has a different way of computing the ice surface temperature than the ERA model.

The corresponding multi-annual seasonal averages of precipitation are shown in Fig. 4. Differences between CRCM5 simulation and CRU TS3.1 and UDEL observation

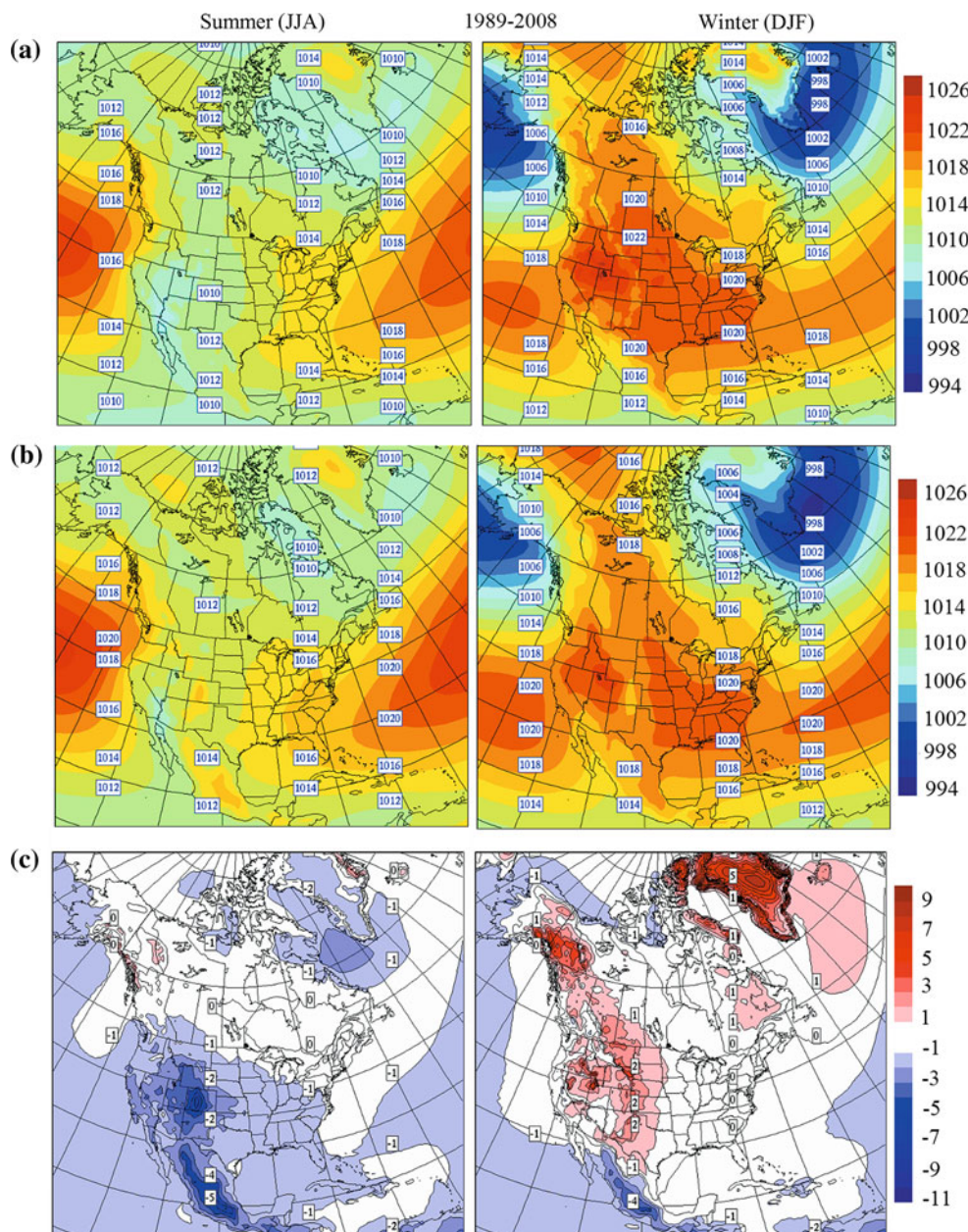


Fig. 2 **a** CRCM5 and **b** ERA-Interim mean JJA (left panels) and DJF (right panels) sea level pressure for the 1989–2008 period. Differences between CRCM5 and ERA-Interim sea level pressures are shown in **(c)**

datasets are presented, both in absolute and relative (in % of mean value between simulation and reference dataset) terms. It can be seen that for almost the whole continent, the absolute difference is within 2 mm/day, with the exception of coastal zones, for both seasons. Most important differences occur over the Northern Pacific Coast in both seasons, and over Mexico and Central American part of the domain, mostly in summer. The relative difference figures show the precipitation bias patterns in more details. In summer, the difference between simulated and observed precipitation does not exceed 25 % for the most part of the

continent. A strong negative relative bias can be seen in the NAM zone in the Southwestern part of the continent in summer; positive bias along the coastal line can be also seen in summer.

In winter, there is a remarkable contrast of relative bias along the Canada–US border, with a weak bias over most part of Canada and substantial positive bias over United States, and this is present in comparisons of CRCM5 simulations with both CRU TS3.1 and UDel data. Because this sharp contrast occurs over a homogenous geoclimatical zone, the Prairies, it deserves some attention. In order to

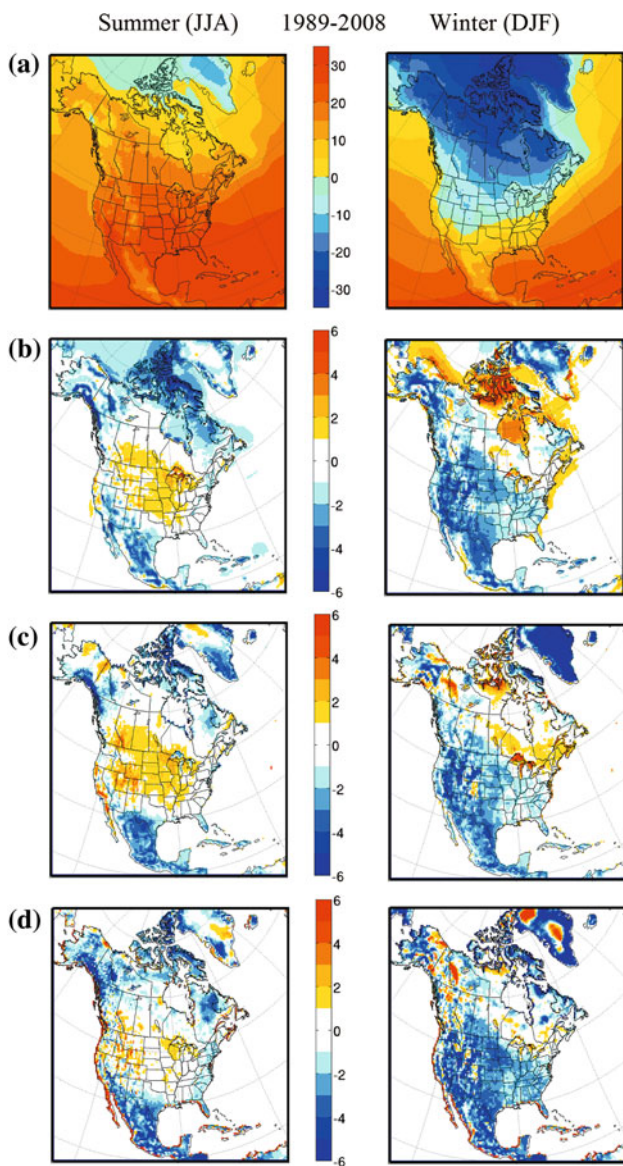


Fig. 3 Comparison of CRCM5 simulated mean JJA and DJF 2-m air temperature (°C) with that of ERA-Interim reanalysis, CRU TS3.1 and UDel datasets, for the 1989–2008 period. **a** CRCM5 2-m air temperature (°C), **b** CRCM5—ERA-Interim 2-m air temperature difference (°C), **c** CRCM5—CRU TS3.1 2-m air temperature difference (°C), **d** CRCM5—UDEL 2-m air temperature difference (°C)

examine this phenomenon, we have used a satellite observation-based dataset, GPCP-1dd (Huffman et al. 2001), unfortunately available only for a shorter period of time (1996–2008). In Fig. 5 comparison of precipitation data, similar to that shown in Fig. 4, is presented, but for the shorter 1998–2008 period; the satellite-based GPCP-1dd data are shown along with CRU TS3.1 and UDel datasets. CRCM5 and GPCP-1dd precipitation and relative

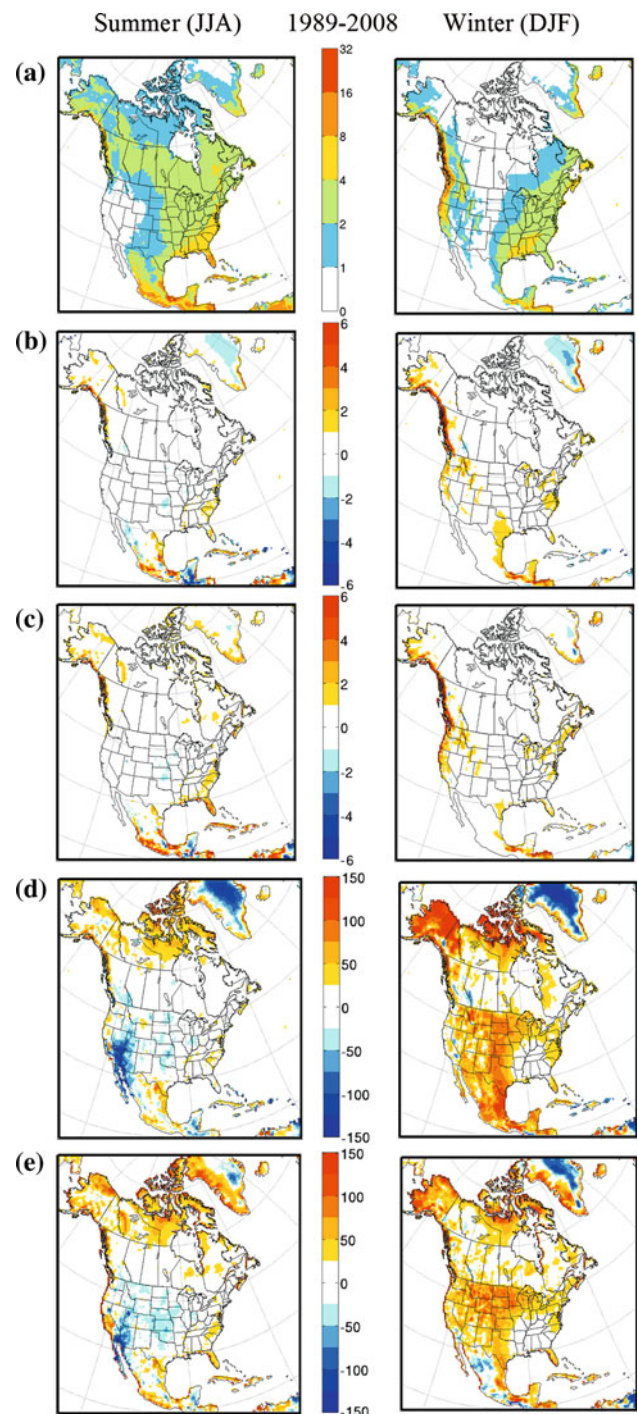


Fig. 4 Comparison of CRCM5 simulated mean JJA and DJF precipitation (mm/day) with CRU TS3.1 and UDel datasets, for the 1989–2008 period. Absolute and relative differences are shown. **a** CRCM5 daily precipitation (mm/day), **b** CRCM5—CRU TS3.1 absolute difference of daily precipitation (mm/day), **c** CRCM5—UDEL absolute difference of daily precipitation (mm/day), **d** CRCM5—CRU TS3.1 relative difference of daily precipitation (%), **e** CRCM5—UDEL relative difference of daily precipitation (%)

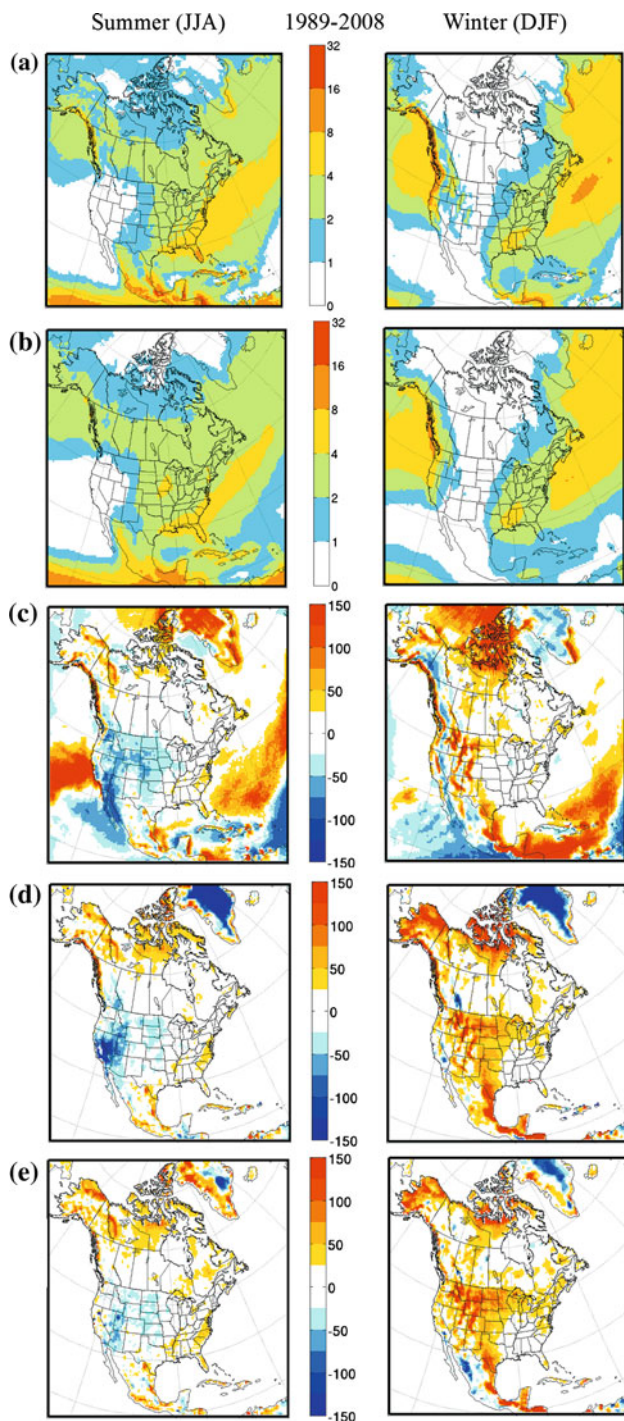


Fig. 5 Comparison of CRCM5 simulated mean JJA and DJF precipitation (mm/day) with GPCP-1dd, CRU TS3.1 and UDeI datasets, for the 1989–2008 period. Relative differences in % are shown in relation to GPCP-1dd dataset. **a** CRCM5 daily precipitation (mm/day), **b** GPCP-1dd daily precipitation (mm/day), **c** CRCM5—GPCP-1dd relative difference of daily precipitation (%), **d** CRCM5—CRU TS3.1 relative difference of daily precipitation (%), **e** CRCM5—UDeI relative difference of daily precipitation (%)

differences in relation to the GPCP-1dd dataset between simulated and observation-based data are shown. As GPCP-1dd data are available over oceans, CRCM5 simulation data over oceans are also presented. It can be seen that the gradient of relative bias of precipitation across the Canada–US border, present in CRU TS3.1 and UDeI winter figures, is absent when the simulation is compared with GPCP-1dd. This feature can supposedly be linked with non-corrected systematic bias in national meteorological observation data, used to generate the CRU TS3.1 and UDeI datasets. Yang et al. (2005) showed that there are noticeable discrepancies in catch efficiency between the national gauges used in Canada and United States. In the GPCP-1dd dataset, where satellite-based data are used along with ground observations and complex data treatment procedure (Adler et al. 2003), the issue of gauge efficiency seems to be resolved. We can thus conclude that the apparent cross-border gradient of precipitation bias is actually an artefact caused by the CRU TS3.1 and UDeI datasets. Similar cross-border gradients can be seen in figure 9 of Mearns et al. (2012). Higher precipitation biases over coastal regions, especially the Pacific Coast, can be explained by difficulties in correctly simulating the precipitation mechanisms in conditions of steep and complex orography. The horizontal grid mesh (0.44°) is not sufficient in such regions, where steep mountain systems are neighbored by oceans, forming complex coastal line. For the same reason the observation and reanalysis data may not be very precise in these regions either. It can be hoped that the quality of reproducing the precipitation patterns in coastal regions will be improved at higher horizontal resolution.

The winter CRCM5 precipitation biases relative to GPCP-1dd over Alaska, the Canadian Arctic Archipelago and Greenland are also lower than those relative to CRU TS3.1 and UDeI. One possible explanation is that the satellite-based GPCP-1dd data have better spatial sampling than ground-based observations in this region.

In summer, the GPCP-1dd—relative precipitation bias is stronger over the Prairies and Southwest. This corresponds to the zone of relatively weak precipitation (less than 1 mm/day over the West Coast, less than 2 mm/day over the Prairies), which in simulation (Fig. 5a) extends eastwards further than in observations (Fig. 5b–e). In such dry zones small absolute biases in precipitation correspond to large relative biases. Some of these regions, in particular the NAM region, will be discussed in more details later in the article.

We will further consider in more details different geoclimatic subregions of the continent and try to reveal the performance of the simulation in more details.

4 Performance on the subdomain level

4.1 1989–2008 climatology by subdomains

The map of relatively homogenous geoclimatic regions is presented in Fig. 6. These regions are based on those developed by Bukovsky (2011), adapted to the CRCM5 simulation grid. In order to reduce the overall number of

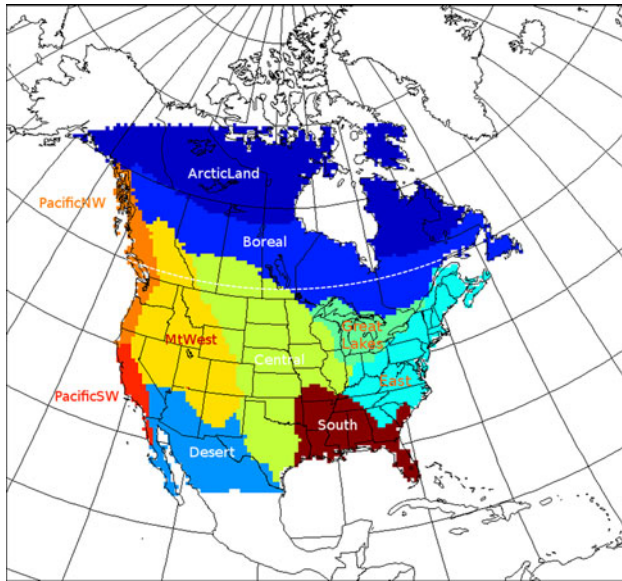


Fig. 6 Subdomains considered in the study (adapted from Bukovsky 2011). The ocean part of the Bukovsky coastal subdomains is not considered. Large Bukovsky regional subdomains are used, where reasonable. The fiftieth parallel North (shown in white dashes) corresponds to the northern limit of TRMM data

regions, the compound Bukovsky subdomains were used, where feasible. In total, 10 subregions will be presented in the article.

The climatology of 2-m air temperature and precipitation for the 1989–2008 period over the Bukovsky subdomains is presented on Tables 2, 3 and 4 for the JJA and DJF seasons and the whole year, respectively. Mean value and interannual standard deviation (IASD) are presented for CRCM5 simulation and for the reference ensemble. The ensemble mean of ERA-Interim, CRU TS3.1 and UDel data were used as reference for the 2-m air temperature, and CRU TS3.1 and UDel ensemble mean values were used as reference for precipitation. The biases and interannual correlation coefficients of annual and seasonal mean values, calculated for every year in the 1989–2008 period, between simulated and reference data are also shown.

The maximum biases between simulation and reference means occur in the Desert subregion: $-1.9\text{ }^{\circ}\text{C}$ for JJA, $-3.0\text{ }^{\circ}\text{C}$ for DJF and $-2.3\text{ }^{\circ}\text{C}$ for the whole year. Maximum precipitation biases occur in the Pacific NW region: 0.7 mm/day for JJA, 2.3 mm/day for DJF, and 1.8 mm/day for the whole year. It can be seen from Table 4 that the annual averaged temperature for most subdomains is slightly underestimated in the CRCM5 simulation, and the average precipitation rates are overestimated by 5–30 %, with exception of the complex Pacific NW subregion (41 %) and of the Arctic Land (45 %) subregion, where an all-year-round wet bias is produced by the model.

The correlation coefficients both for 2-m air temperature and for precipitation are noticeably lower in summer than in winter. This might be related to convective nature of summer precipitation, difficult to simulate, as noted earlier

Table 2 CRCM5-simulated and observation-based 2-m air temperature and precipitation for summer (JJA), 1989–2008

Subdomain	2-m air temperature, $^{\circ}\text{C}$						Precipitation, mm/day					
	CRCM5		Reference		Bias	<i>r</i>	CRCM5		Reference		Bias	<i>r</i>
	Mean	IASD	Mean	IASD			Mean	IASD	Mean	IASD		
Arctic Land	8.8	1.3	10.3	0.6	-1.5	0.30	2.1	0.2	1.7	0.1	0.4	0.71
Boreal	14.8	1.0	15.0	0.7	-0.2	0.61	2.8	0.3	2.6	0.2	0.2	0.56
Central	23.1	1.0	22.4	0.8	0.8	0.79	2.1	0.5	2.4	0.3	-0.3	0.75
Desert	25.3	0.6	27.2	0.6	-1.9	0.43	1.6	0.3	1.6	0.3	0.0	0.16
East	21.3	0.6	21.6	0.6	-0.3	0.67	3.7	0.6	3.5	0.5	0.2	0.43
Great Lakes	20.1	0.9	19.2	1.0	0.9	0.71	2.6	0.6	2.7	0.3	0.1	0.23
Mt. West	18.5	1.2	18.0	0.8	0.5	0.77	0.9	0.2	1.0	0.2	-0.1	0.86
Pacific NW	12.4	1.0	13.5	0.6	-1.1	0.74	2.8	0.5	2.1	0.3	0.7	0.65
Pacific SW	22.6	1.0	21.9	0.6	0.7	0.48	0.14	0.13	0.17	0.12	-0.03	0.68
South	26.9	0.7	26.9	0.6	0.0	0.60	4.5	0.7	4.1	0.7	0.4	0.18

Statistics of climatological JJA means and interannual standard deviation (IASD), as well as bias and interannual anomaly correlation coefficient *r* are shown, with statistically significant (CI 95 %, $p < 0.05$) correlation coefficients in bold. Reference datasets: ERA-Interim, CRU TS3.10 and UDel for temperature, CRU TS3.10 and UDel for precipitation

Table 3 CRCM5-simulated and observation-based 2-m air temperature and precipitation for winter (DJF), 1989–2008

Subdomain	2-m air temperature, °C						Precipitation, mm/day					
	CRCM5		Reference		Bias	<i>r</i>	CRCM5		Reference		Bias	<i>r</i>
	Mean	IASD	Mean	IASD			Mean	IASD	Mean	IASD		
Arctic Land	−23.9	1.7	−23.7	1.7	−0.2	0.82	1.0	0.1	0.7	0.1	0.3	0.69
Boreal	−15.7	1.5	−15.5	1.7	−0.2	0.89	1.5	0.1	1.2	0.1	0.3	0.55
Central	−5.2	1.5	−2.7	1.6	−2.5	0.90	1.3	0.2	0.8	0.1	0.5	0.78
Desert	8.5	0.7	11.5	0.7	−3.0	0.88	0.8	0.4	0.6	0.3	0.2	0.88
East	−0.8	1.5	−0.3	1.4	−0.5	0.91	3.6	0.7	2.9	0.4	0.7	0.63
Great Lakes	−4.7	1.7	−5.1	1.7	0.4	0.91	2.5	0.4	1.7	0.3	0.8	0.77
Mt. West	−5.6	1.2	−3.0	1.0	−2.6	0.86	1.8	0.3	1.2	0.2	0.6	0.88
Pacific NW	−2.3	1.1	−1.1	1.0	−1.2	0.91	8.5	1.0	6.2	0.9	2.3	0.90
Pacific SW	6.8	0.9	8.8	0.8	−2.0	0.93	3.7	1.5	3.1	1.1	0.6	0.94
South	8.3	1.1	9.6	0.9	−1.3	0.79	3.6	0.4	3.5	0.7	0.1	0.79

Statistics of climatological DJF means and interannual standard deviation (IASD), as well as bias and interannual anomaly correlation coefficient *r* are shown, with statistically significant (CI 95 %, $p < 0.05$) correlation coefficients in bold. Reference datasets: ERA-Interim, CRU TS3.10 and UDel for temperature, CRU TS3.10 and UDel for precipitation

Table 4 CRCM5-simulated and observation-based 2-m air temperature and precipitation for the whole year, 1989–2008

Subdomain	2-m air temperature, °C						Precipitation, mm/day					
	CRCM5		Reference		Bias	<i>r</i>	CRCM5		Reference		Bias	<i>r</i>
	Mean	IASD	Mean	IASD			Mean	IASD	Mean	IASD		
Arctic Land	−7.8	0.8	−6.7	0.9	−1.1	0.77	1.6	0.1	1.1	0.04	0.5	0.51
Boreal	−0.3	0.8	0.4	0.9	−0.7	0.87	2.2	0.1	1.8	0.1	0.1	0.60
Central	8.9	0.7	10.0	0.7	−1.1	0.90	1.9	0.2	1.6	0.1	0.3	0.64
Desert	17.3	0.4	19.6	0.4	−2.3	0.85	1.0	0.2	0.9	0.1	0.1	0.68
East	10.2	0.5	10.8	0.6	−0.6	0.91	3.8	0.3	3.2	0.3	0.6	0.55
Great Lakes	7.6	0.8	7.3	0.8	0.3	0.90	2.9	0.3	2.3	0.2	0.6	0.34
Mt. West	6.0	0.5	7.3	0.4	−1.3	0.74	1.4	0.2	1.1	0.1	0.3	0.94
Pacific NW	4.7	0.5	6.0	0.5	−1.3	0.82	6.1	0.5	4.3	0.4	1.8	0.90
Pacific SW	14.6	0.4	15.3	0.4	−0.7	0.58	1.6	0.5	1.4	0.4	0.2	0.95
South	17.7	0.5	18.4	0.5	−0.7	0.83	3.9	0.4	3.7	0.4	0.2	0.62

Statistics of annual climatological means and interannual standard deviation (IASD), as well as bias and interannual anomaly correlation coefficient *r* are shown, with statistically significant (CI 95 %, $p < 0.05$) correlation coefficients in bold. Reference datasets: ERA-Interim, CRU TS3.10 and UDel for temperature, CRU TS3.10 and UDel for precipitation

by other authors (e.g., Plummer et al. 2006; Jiao and Caya 2006).

As a general rule, interannual correlation coefficients exceeding 0.55–0.6 are statistically significant at 95 % CI (shown in bold in Tables 2, 3, 4). Lower correlation values are in most cases statistically insignificant, which means that for these regions and variables the interannual variability remains largely unresolved by the CRCM5 model.

The interannual correlation coefficients between precipitation and 2-m temperature values for CRCM5 data and the reference base of Tables 2, 3 and 4 are presented in Fig. 7 for summer and winter periods. In most cases the signs and values of correlation coefficients in simulations

are close to those in observation data. Exceptions are Arctic Land in JJA and Boreal in DJF. The signs of JJA and DJF correlations are in good agreement with similar results, presented by Mearns et al. (2012), and the correspondence between simulated and reference correlations is consistent with that of NARCCAP models presented in that article. The correlation coefficients between the biases of simulated precipitation and 2-m temperature from corresponding reference values are presented as hollow diamonds in Fig. 7. In summertime the bias correlations are positive in the North of the continent (Arctic Land, Boreal), in the Central subdomain and along the Pacific coast, while the correlations between temperature and precipitation

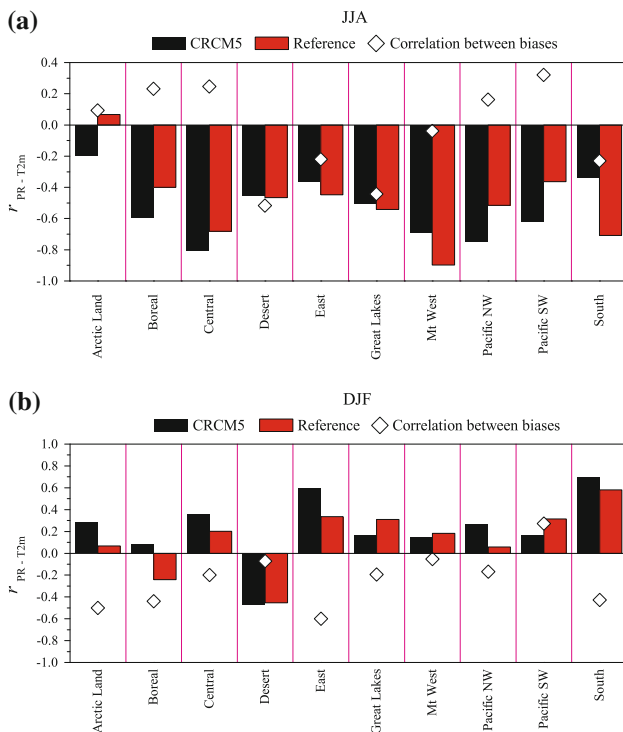


Fig. 7 Interannual correlation coefficients between precipitation and 2-m temperature in CRCM5 simulation (black bars) and the reference base of ERA-Interim, CRU TS3.10 and UDel for temperature, CRU TS3.10 and UDel for precipitation (red bars): **a** JJA, **b** DJF. Hollow diamonds show the correlation coefficients between the biases of simulated precipitation and 2-m temperature values from corresponding reference values

values, presented by color bars, are negative in these regions. In the rest of the continent the bias correlations are positive and close to those presented by color bars. In wintertime in most subdomains the signs of bias correlations and of color bars are opposite to each other, so that the 2-m temperature and precipitation biases are negatively correlated in all subdomains, except in Pacific SW.

4.2 Reproduction of temperature and precipitation: analysis by subregions

Figures 8, 9, 10, 11, 12, 13, 14, 15, 16 and 17 will show, for each subregion, the annual cycle of 2-m air temperature and precipitation, consisting of monthly means averaged over the 20-year-long 1989–2008 period. Simulated data will be compared with the same observation-based data as in the previous section: ERA-Interim, CRU TS3.1 and UDel for temperature, CRU TS3.1 and UDel for precipitation data. Along with multi-annual averaged monthly temperature and precipitation values (connected with lines), the interannual variability of monthly means is shown (boxes and whiskers). For all subregions, distributions of daily precipitation intensities for all tiles within

subdomains, binned over intervals 0, 0.1 and 2^n mm/day, where $n = -2, -1, 0, 1, 2$, etc., are shown for summer (JJA) and winter (DJF) seasons for the 2001–2008 period. In fact, the data should rather be shown as histograms, but they are shown as curves to ease the comparison of different data. The sum of all the bins gives the average precipitation (in mm/day) for the season and the region. For all presented datasets and seasons considered, the following data are printed in the figures: percent number of dry events (i.e. days with precipitation less than 0.1 mm/day), average (for all days, dry and wet) and maximum daily precipitation (mm/day), along with the 99th precipitation percentile for daily precipitations exceeding 1 mm/day (Pq99). CRCM5-simulated precipitation statistics are compared with GPCP-1dd data, and for all subregions located to the south of 50°N and for southern parts of Central, Pacific NW and Mt. West subregions, TRMM data is also used. For ease of comparison, GPCP-1dd and TRMM data were first interpolated on the CRCM5 grid, using the nearest neighbour method. The CRCM5 hourly and TRMM 3-hourly cumulative precipitations were cumulated over 24-h periods, while daily GPCP-1dd data were used directly.

The subregion Arctic Land represents the taiga and tundra regions, and corresponds to the combination of Bukovsky’s subregions East Taiga, West Taiga, East Tundra, Central Tundra and West Tundra. Arctic Land roughly corresponds to the Köppen ET (tundra) and EF (ice cap) climate areas of the North American continent, with polar tundra and taiga being the main vegetation types. The Arctic Land subregion does not include the Canadian Arctic Archipelago and most part of Alaska where substantial differences between observation and simulation data, as well as between different observation datasets are present (see previous Section). The observation and simulation results, presented in Fig. 8, are in accordance with Köppen classification. The average annual temperature is evidently below 0 °C, with averaged annual maximum in July at around 10 °C and minimum in January at around -26 °C. The interannual variability of CRCM5 monthly mean values of 2-m air temperature is higher than in observations in summertime, and comparable with observations in other periods of the year. There is good general agreement between simulation data and observations, with differences smaller than the interannual variability, except in summertime when a weak cold bias (1–2 °C) can be noticed. The precipitation over the Arctic Land subregion is overestimated in simulations by 0.25–1 mm/day. The shape of the annual cycle, however, is well reproduced, with a precipitation minimum in winter and early spring (January–March) and maximum in summertime. The simulated precipitation maximum is reached in September instead of July–August in observations. The interannual

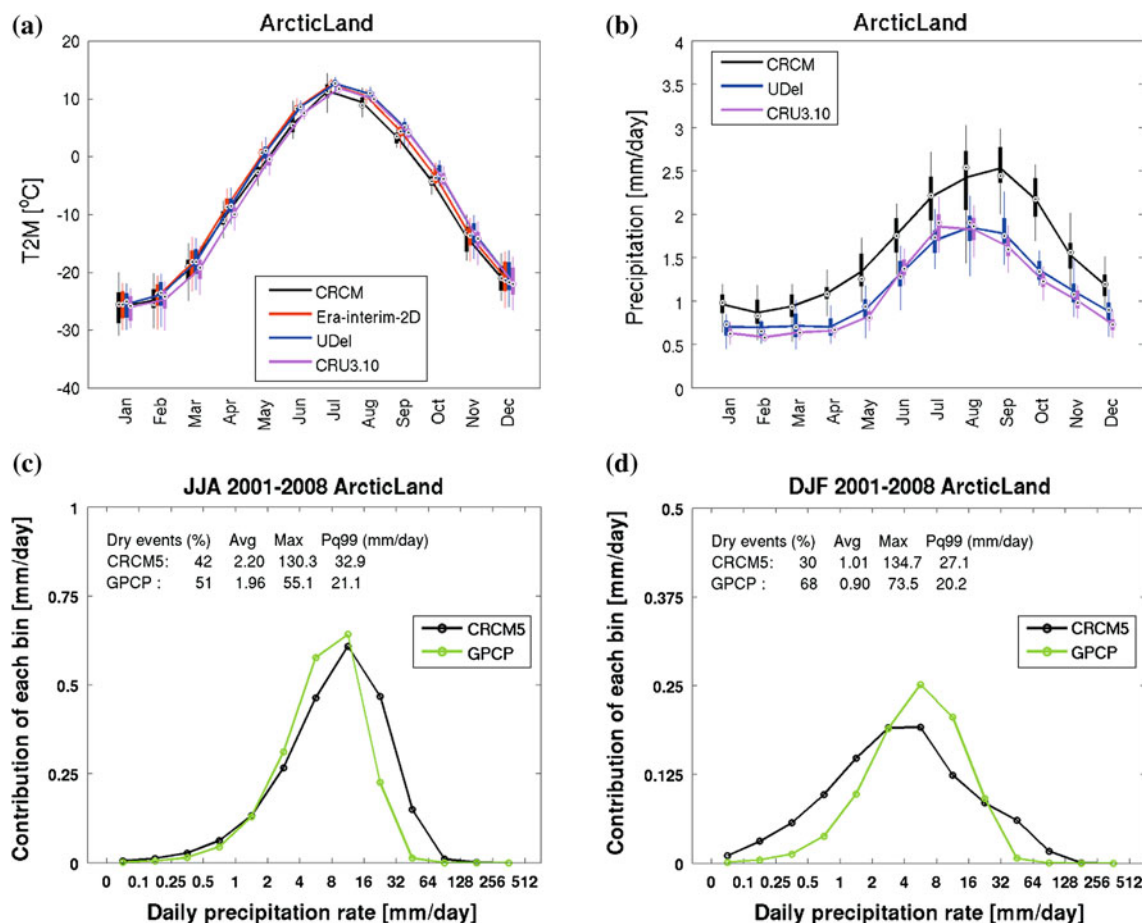


Fig. 8 CRCM5 simulated and observed mean a 2-m air temperature ($^{\circ}\text{C}$) and **b** precipitation (mm/day) annual cycles along with the interannual variability of monthly means (*boxes* and *whiskers*) for the Arctic Land subdomain; the white “targets” denote the median values, *lower* and *upper box* limits denote the 25th and 75th percentile, respectively, while *whiskers* indicate the extreme data (outliers, i.e. values exceeding 1.5 times the inter-quartile range, are

variability of CRCM5-simulated precipitation and temperature is comparable with that of observations in wintertime and exceeds them in summertime.

The frequency distributions of daily precipitation in the CRCM5 simulations and in the GPCP-1dd data are notably different in winter (Fig. 8d). The bell-shaped precipitation distribution is wider and lower in the CRCM5 simulation than in the GPCP-1dd data: relatively more low-precipitation and high-precipitation events were produced by the model in comparison with observation-based data. The number of dry events in simulation is however remarkably lower than in GPCP-1dd (30 % in the model vs. 68 % in observations). The 99th percentile in CRCM5 data is shifted towards higher precipitation rates. In summertime, the precipitation frequency distribution has a maximum at the 8–16 mm/day bin in the model and observations (Fig. 8c). The percent number of dry events is also similar:

not shown). The *bottom panel* shows CRCM5 and GPCP-1dd frequency distributions of daily **c** summer and **d** winter precipitation for the 2001–2008 period, for the subdomain. The percent number of dry events (i.e. days with precipitation below 0.1 mm/day), average and maximum daily precipitation and the 99th percentile (mm/day) are also indicated in the (c) and (d)

42 % in CRCM5 simulation and 51 % in GPCP-1dd. The CRCM5 distribution is slightly shifted towards higher daily precipitation rates compared with GPCP-1dd data, which is consistent with higher 99th percentile CRCM5 value.

The Boreal subregion combines two Bukovsky subdomains, EBoreal and WBoreal, and corresponds mostly to Köppen climates EF (ice cap climate) and Dfb (hemiboreal temperate climate). This region corresponds in general to a wide band of boreal conifer and mixed forests, spread across the northern part of the continent, from northern Rocky Mountains to the Atlantic coast of Québec and Newfoundland and Labrador. The annual cycles of air temperature and precipitation for this subregion are shown in Fig. 9. The simulated air temperature cycle is consistent with observations; the difference between the CRU TS3.1 and other observation datasets exceeds that between simulated data and observation datasets. The typical

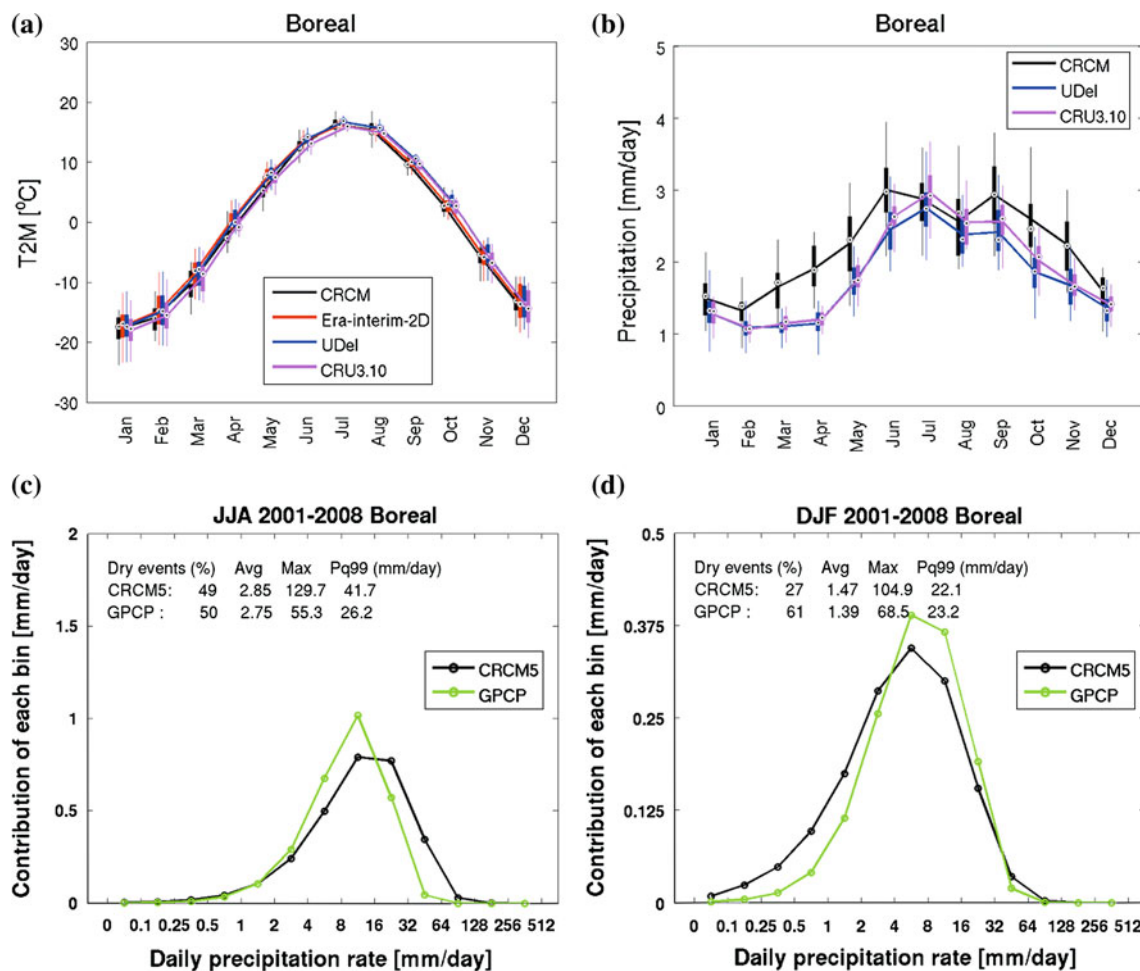


Fig. 9 Same as Fig. 8, but for the Boreal subdomain

continental annual temperature cycle with minimum temperature in January (around $-18\text{ }^{\circ}\text{C}$) and maximum in July (around $15\text{ }^{\circ}\text{C}$) can be seen in Fig. 9a. As in the Arctic Land subregion, the interannual variability of monthly means in simulation data is higher than that of observations in summer and comparable in other seasons. The precipitation annual cycle, with a maximum in summertime and a minimum in winter, is in general reproduced by the CRCM5. In summer and in winter the simulated and observed precipitation rates are comparable. However, during transitional seasons the simulated precipitation is overestimated compared to observations. The excess of precipitation reaches its maximum of around 1 mm/day in April and around 0.5 mm/day in October in autumn. Note the strong interannual variability of both simulation and observation precipitation. The precipitation distribution in the CRCM5 simulation is close to observations both in winter and in summertime. In winter season, higher fraction of CRCM5 precipitation is produced by low-precipitation events than in GPCP-1dd data; in summertime, there

is a weak bias in simulated precipitation distribution towards higher precipitation rates.

The Central subregion regroups the CPlains, NPlains, SPlains and Prairies basic subregions of Bukovsky. It encloses the areas with the Köppen climate types Dfb (hemiboreal), Dfa (hot summer continental), BSk (mid-latitude steppe) and CFa (humid subtropical with uniform precipitation distribution). While different climate types are present over this large subregion, it is representing relatively homogenous landscapes of Great Plains and Prairies. The temperature and precipitation patterns for this subregion are presented in Fig. 10. The annual 2-m air temperature cycle shows a cold winter bias of CRCM5, which is also visible in Fig. 3. In summer a weak warm bias can be noted, comparable to differences between observation datasets. The maximum temperature of around $23\text{ }^{\circ}\text{C}$ is reached in July and the minimum (-5 to $-7\text{ }^{\circ}\text{C}$) in January. The interannual variability of monthly means is similar in observations and in simulation data over the whole annual cycle. The precipitation cycle, with winter

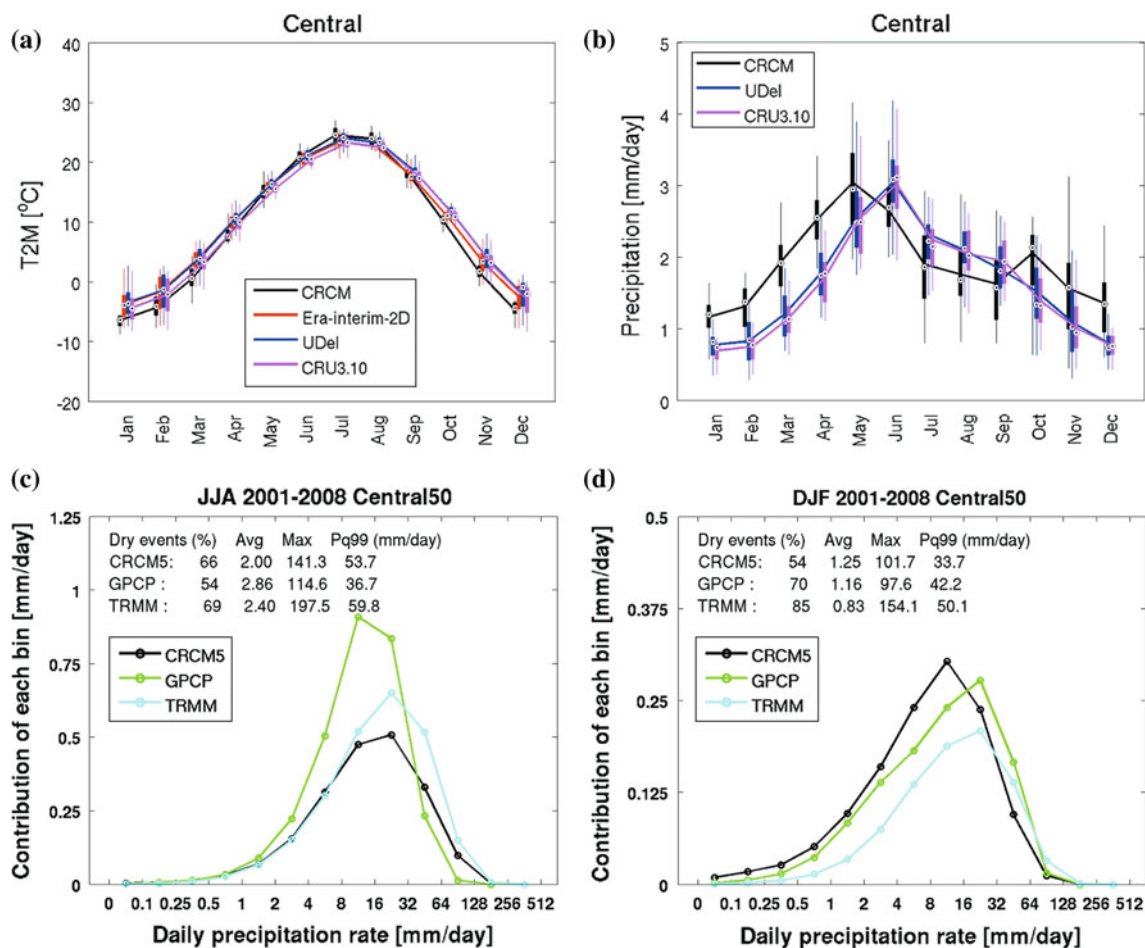


Fig. 10 Same as Fig. 8, but for the Central subdomain; the TRMM data are shown along with CRCM5 and GPCP on panels **c** and **d**

minimum and summer maximum, is reproduced by the simulation in general, although the precipitation rate is overestimated by nearly 1 mm/day in winter and spring, and is underestimated in summer and in early autumn by 0.5 mm/day. Differences between observation datasets are considerable in summer (Fig. 10c), where GPCP-1dd average summer precipitation exceeds that of CRCM5 and TRMM and its distribution is shifted towards lower daily precipitation values. In wintertime the CRCM5-simulated precipitation distribution is in general similar to observational data, although the CRCM5 distribution is slightly shifted towards lower daily precipitation rates (Fig. 10d). There is noticeable difference between TRMM and GPCP-1dd data both in winter and in summer, concerning the total average daily precipitation, frequency distributions, 99th percentiles and the number of dry events. The possibility of such an important discrepancy between two observation-based datasets makes us to restrict the comparison of simulation data with observations to most general features.

The Great Lakes area, one of the basic Bukovsky subregions, is dominated by Köppen's continental (Dfa, Dfb)

climate types. The Laurentian Great Lakes cover almost 50 % of its area. In CRCM5 simulation, the interactively-coupled 1D Flake model is used to reproduce the water temperature, ice fraction, thickness and temperature over lakes; thus, the quality of reproducing the climate of this subregion depends strongly on the performance of the coupled lake model. As it can be seen in Fig. 11, the averaged 2-m air temperature is in general reproduced over the whole annual cycle; the simulated temperature is warmer than that of the reference datasets in summertime. However, Fig. 3 suggests that this result is actually due to compensating biases over lakes and surrounding land area. It is known (Martynov et al. 2012) that the FLake model overestimates the summer temperature of deep Great Lakes and leaves the water free of ice longer than observed, thus creating a warm bias in winter. There is also a notable distinction of CRU TS3.1 temperature data in wintertime from other datasets. The precipitation cycle, according to observations, has a weak maximum in summertime; average precipitation rate decreases slowly towards the minimum in February. The precipitation rate is well reproduced

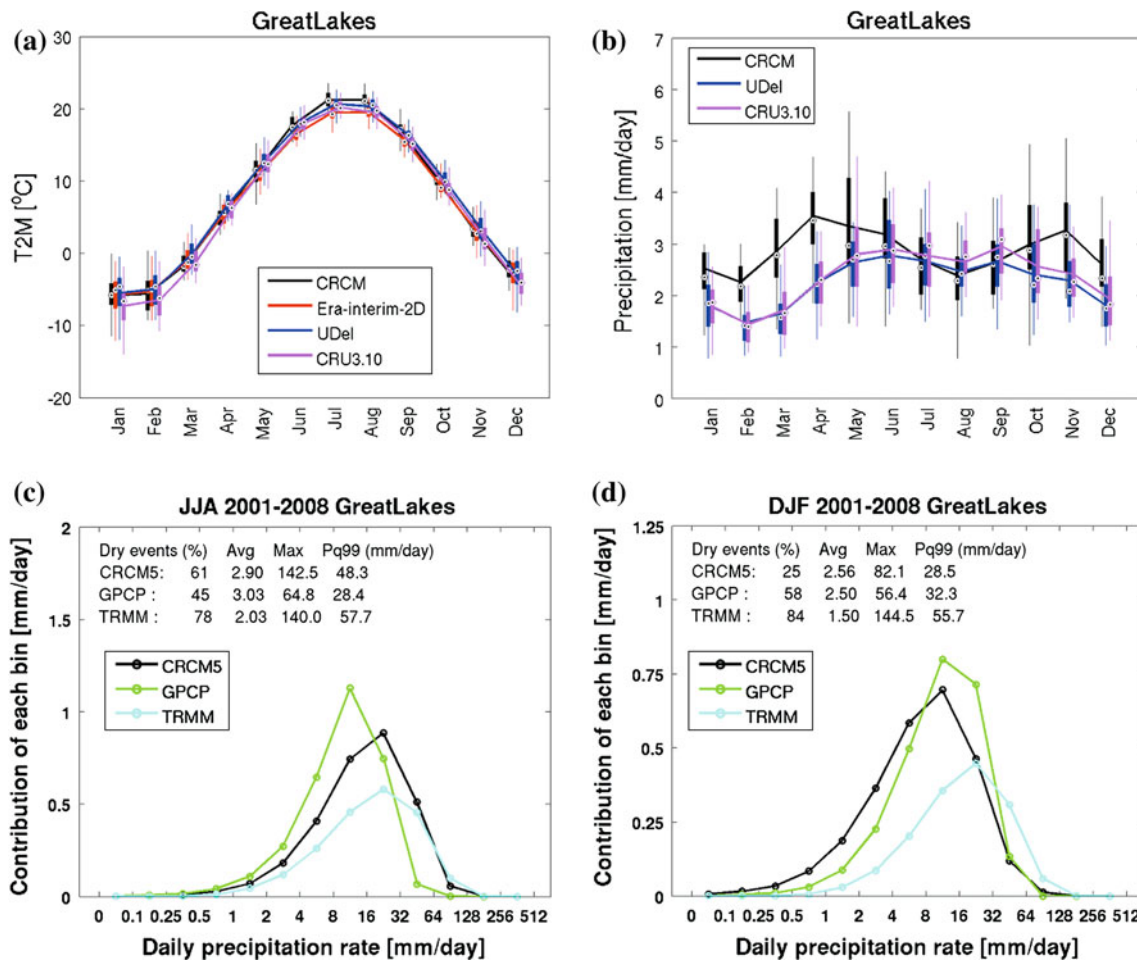


Fig. 11 Same as Fig. 10, but for the Great Lakes subdomain

by the model in summertime, while for the rest of the annual cycle it is overestimated by 0.7–1.2 mm/day. During autumn and winter months excess precipitation can supposedly be explained by enhanced evaporation from the overly warm ice-free surface of the Great Lakes in CRCM5. The interannual variability of precipitation rates is high in simulation and observation-based data, thus the statistical significance of differences is questionable. In summertime, the precipitation distribution in CRCM5 simulation is in between TRMM and GPCP-1dd data (Fig. 11c); its shape resembling mostly that of TRMM data. GPCP-1dd data are shifted towards lower daily precipitation rates. The precipitation distribution in winter (Fig. 11d) demonstrates the relative abundance of low-precipitation events in CRCM5 data, supporting the hypothesis of lake evaporation-enhanced precipitation. This is however not seen in observation-based data.

Three basic Bukovsky subdomains, Appalachia, Mid Atlantic and North Atlantic, were grouped to make the East subregion, where continental (Dfa, Dfb) and humid subtropical (Cfa) Köppen climate zones are prevailing. The

temperature and precipitation cycles for this subdomain are presented in Fig. 12. A small negative bias of simulated 2-m air temperature is present in autumn; it is comparable with interannual variability of both observation and simulation data. In other seasons, the average simulated 2-m air temperature is very close to observation values. The annual precipitation cycle is flat, without pronounced difference between seasons, both in observation and simulation data. The simulation overestimates the precipitation by 0.5–1.0 mm/day, except in summertime, where the wet bias almost vanishes. The interannual variability is strong both in the observation-based datasets and in the CRCM5 simulation data. In summer the CRCM5 precipitation frequency distribution is close to that of GPCP-1dd, which is however slightly shifted towards low precipitation rates (Fig. 12c). TRMM average daily precipitation is low in relation to other datasets; however, in summer the precipitation frequency distribution shapes of CRCM5 and TRMM are close, including the 99th percentile values, with GPCP data shifted towards lower precipitation rates. In winter the precipitation frequency distributions of CRCM5

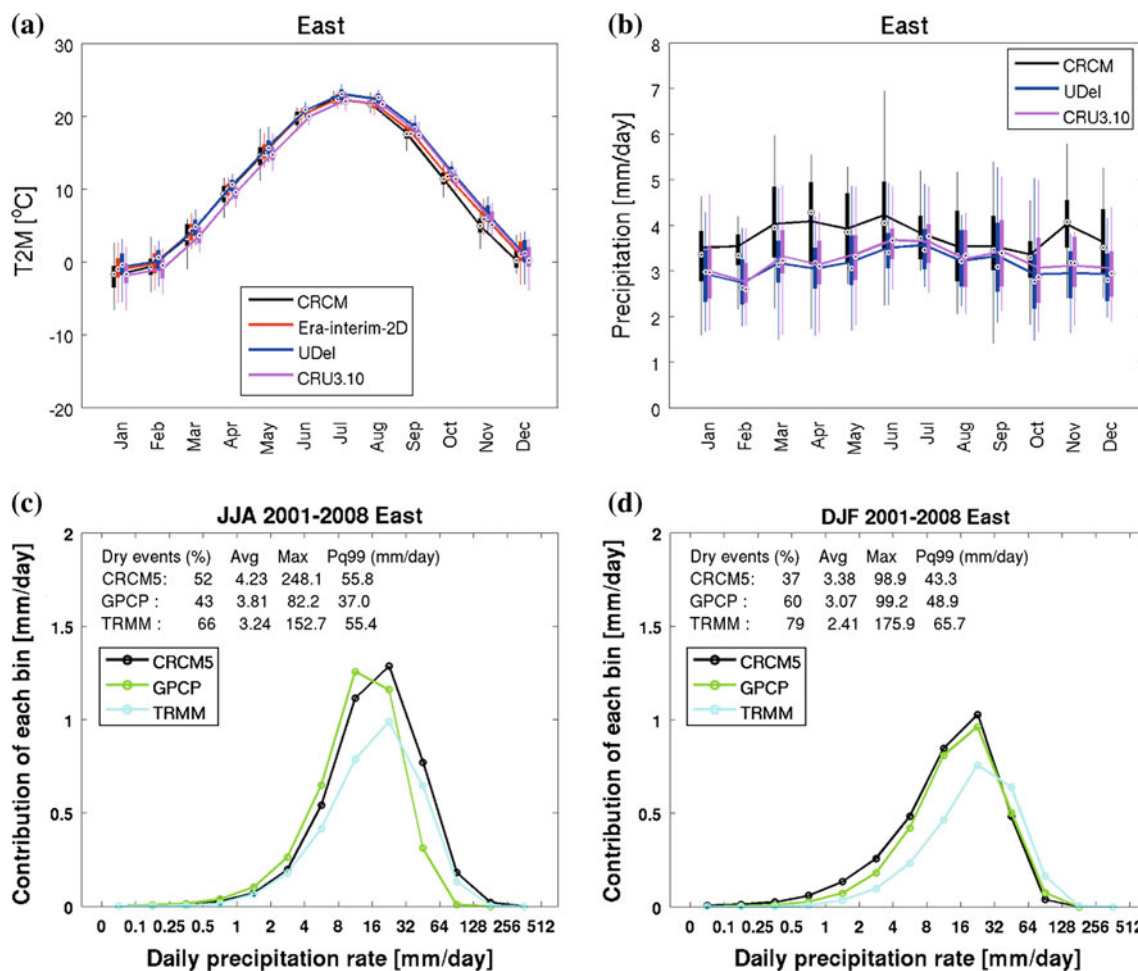


Fig. 12 Same as Fig. 10, but for the East subdomain

and GPCP-1dd are very close, and the TRMM data are slightly biased towards higher precipitation intensities.

The South subregion consists of Southeast and Deep South basic Bukovsky subregions. It is entirely covered by the Cfa (humid subtropic) Köppen climate type. As shown in Fig. 13, there is a small negative bias of 2-m air temperature in winter, while during the rest of the year, the simulated temperature is fairly close to observation-based data. The flat precipitation cycle is well reproduced and the differences between observed and simulated precipitation multi-annual averages are small in comparison with strong interannual variability. The precipitation distribution in summertime demonstrates good coincidence with observation-based data (Fig. 13c), especially with the TRMM database. In winter, the 99th percentile value of CRCM5 is considerably lower than those of both observation datasets: the model produces less high precipitation rate events than observed in this region, because the simulated precipitations are biased towards lower precipitation ratios (Fig. 13d). The daily precipitation rates are high in comparison to all other subregions of this study; there are

relatively few precipitation events with daily precipitation rates lower than 1 mm/day. However, the percentage number of dry events is relatively high, 50–78 % in winter and 44–58 % in summertime.

The Mt. West is constituted of N Rockies, S Rockies and Great Basin basic Bukovsky subregions, thus covering the most part of mountainous areas of the Western North America. Because of complex orography and vast geographical extent, various climate types are presented in this subdomain: Bsk (arid steppe climate, prevailing), Bwk, Bwh (arid desert), Dfb, Dsa (continental), and Cwb (temperate with dry winters). As shown in Fig. 14, the strong annual cycle of 2-m air temperature is reproduced by the CRCM5 with notable cold bias in wintertime, reaching approximately 4 °C. This is the largest temperature bias for all subdomains of the continent presented in this article. The cold bias reaches its maximum in December and vanishes between April and September. The interannual variability of temperature data is relatively small. The precipitation annual cycle is weakly pronounced, according to observations. However, in CRCM5 simulation there is a

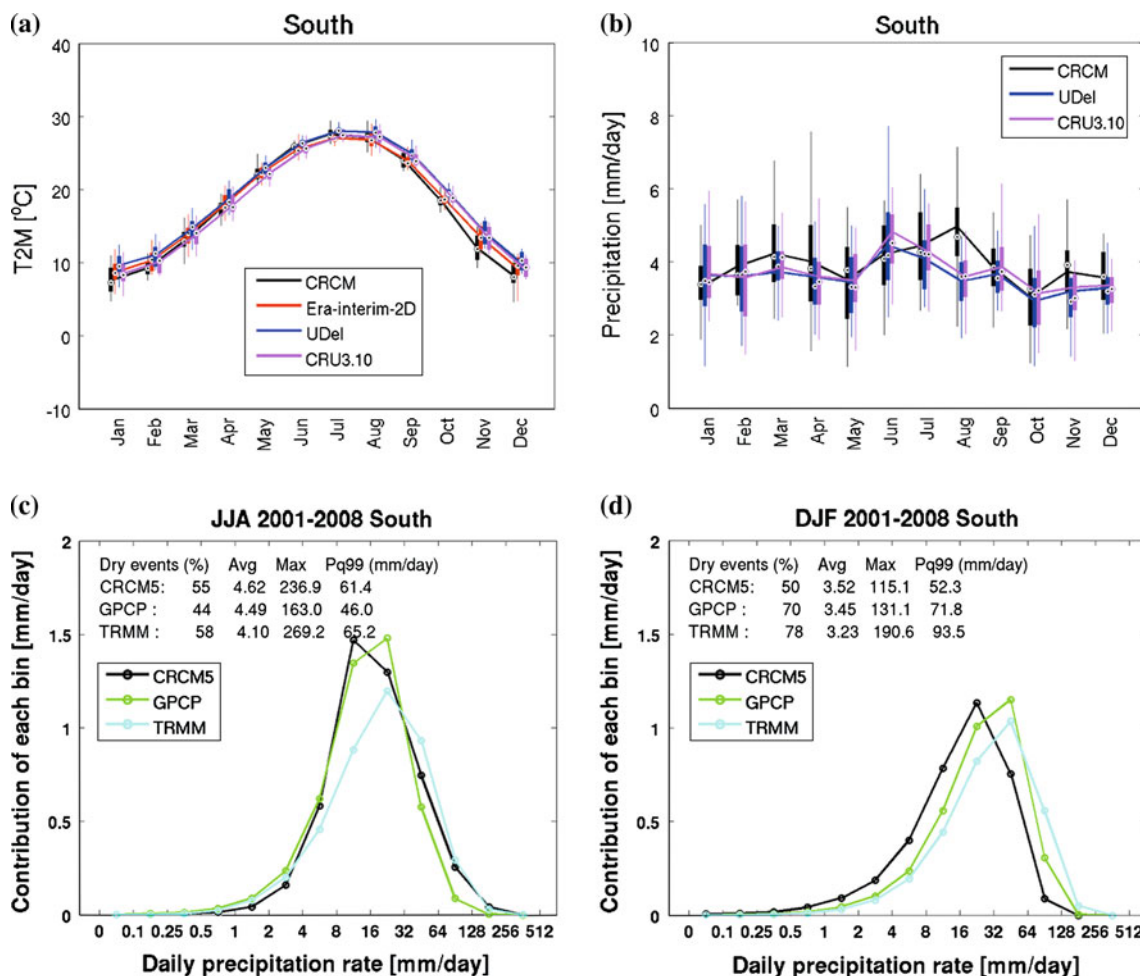


Fig. 13 Same as Fig. 10, but for the South subdomain

strong precipitation minimum in summertime (July–September), when it drops 0.2–0.3 mm/day below observation data; during the rest of the annual cycle the precipitation is overestimated by 0.3–0.5 mm/day. The simulated precipitation annual cycle resembles rather that of the Pacific NW region, shown below. Both in summer and in winter the shapes of simulated and observed precipitation distribution are quite similar; the average daily precipitation however is underestimated in summer (Fig. 14c) and overestimated in wintertime (Fig. 14d) in comparison with both reference datasets.

The mountainous regions are particularly difficult for climate models because of high elevations and complex orography, presence of steep slopes, etc. Complex land-surface parameterization schemes are used in CRCM5 (see Sect. 2); however, the quality of reproducing the climate of mountainous regions still represents a serious challenge. Improvement of simulation results can be expected with better horizontal resolution and correspondingly improved topography. It is also important to mention that the adequacy of the observing network in such complex and

inhomogeneous areas, and its gridding with meshes of 0.5° and coarser is questionable and it is reasonable to expect that observation-based datasets are more prone to biases in such complex regions. McPhee and Margulis (2005) have shown that the GPCP-1dd data correlation with the North American Land Data Assimilation System (LDAS), based on high density (12,000–15,000) daily precipitation gauge readings and on Doppler radar precipitation measurements (Cosgrove et al. 2003), is at lowest among four large subdomains of continental USA ($r = 0.56$ for the annual cycle) and that the winter precipitation data are more scattered than those for other seasons.

The Pacific NW subregion is a basic subregion of Bukovsky, corresponding to Köppen oceanic climate types Csb and Cfb. Indeed, Fig. 15 shows mild temperature variations over the annual cycle, reproduced by the CRCM5 model with a cold bias in autumn and winter, and characteristic precipitation annual cycle with dry summer and abundant winter precipitation. The shape of annual precipitation cycle is well reproduced by the model, although there is a wet bias, reaching a maximum in

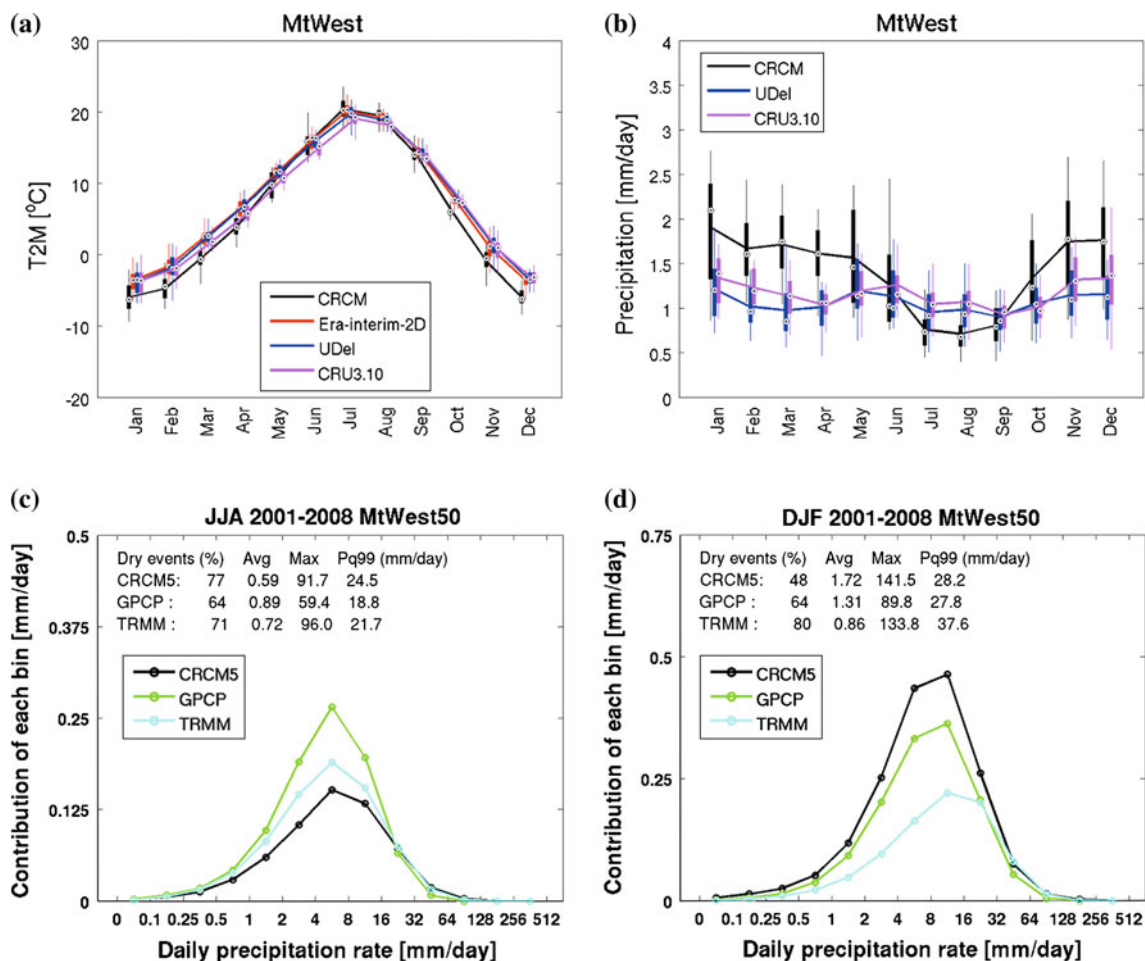


Fig. 14 Same as Fig. 10, but for the Mt. West subdomain

November–January (~ 3 mm/day) and almost vanishing in summertime. The precipitation distribution of the simulation data is close to GPCP-1dd observations in summer (Fig. 15c) with GPCP-1dd data slightly shifted towards low precipitation rates both in summer and in winter (Fig. 15d). This is consistent with the findings of McPhee and Margulis (2005) that high intensity precipitation events (3 mm/day and higher) are partially missing in this dataset in comparison with LDAS daily precipitation values over Pacific Coast north of 40°N .

Pacific NW is a complex subregion, where the Pacific Ocean meets the steep and high Rocky Mountains, with complex coastline, rich with islands and straits. The ability of the CRCM5 model to reproduce correctly the annual precipitation cycle, despite a wet bias in winter, is noteworthy. It can be expected that better results will be obtained at higher horizontal resolution. As the winter precipitations are brought to the region by westerly winds blowing from the ocean, the winter precipitations strongly depend on the correctness of reproduction of these winds by the model. Because of closeness of the domain limit, it

is strongly influenced by the boundary driving conditions; biased driving data could drastically deteriorate the quality of climate simulation along the Pacific Coast. As in the case of Mt. West subregion, the observation-based datasets are prone to errors over the Northern Pacific Coast: McPhee and Margulis (2005) have shown that the correlations between GPCP-1dd and “ground truth” LDAS daily precipitation data are very low ($r = 0.21$ for the annual cycle) over this region.

Over the Pacific SW region, Csb and Csa (dry-summer subtropical) as well as BWk and BWh (arid desert) Köppen climate types are present. As shown in Fig. 16, the relatively mild 2-m air temperature annual cycle is reproduced by the CRCM5 model with a small cold bias in wintertime: the shape of the precipitation cycle with a very dry summer and relatively wet winter is also well reproduced, with the maximum bias of around 1 mm/day in January–February. The interannual variability is strong, compared with multi-annual average values, both in observation and simulation data. In summer (Fig. 16c), when the typical daily precipitation amounts are very small (~ 0.03 mm per day),

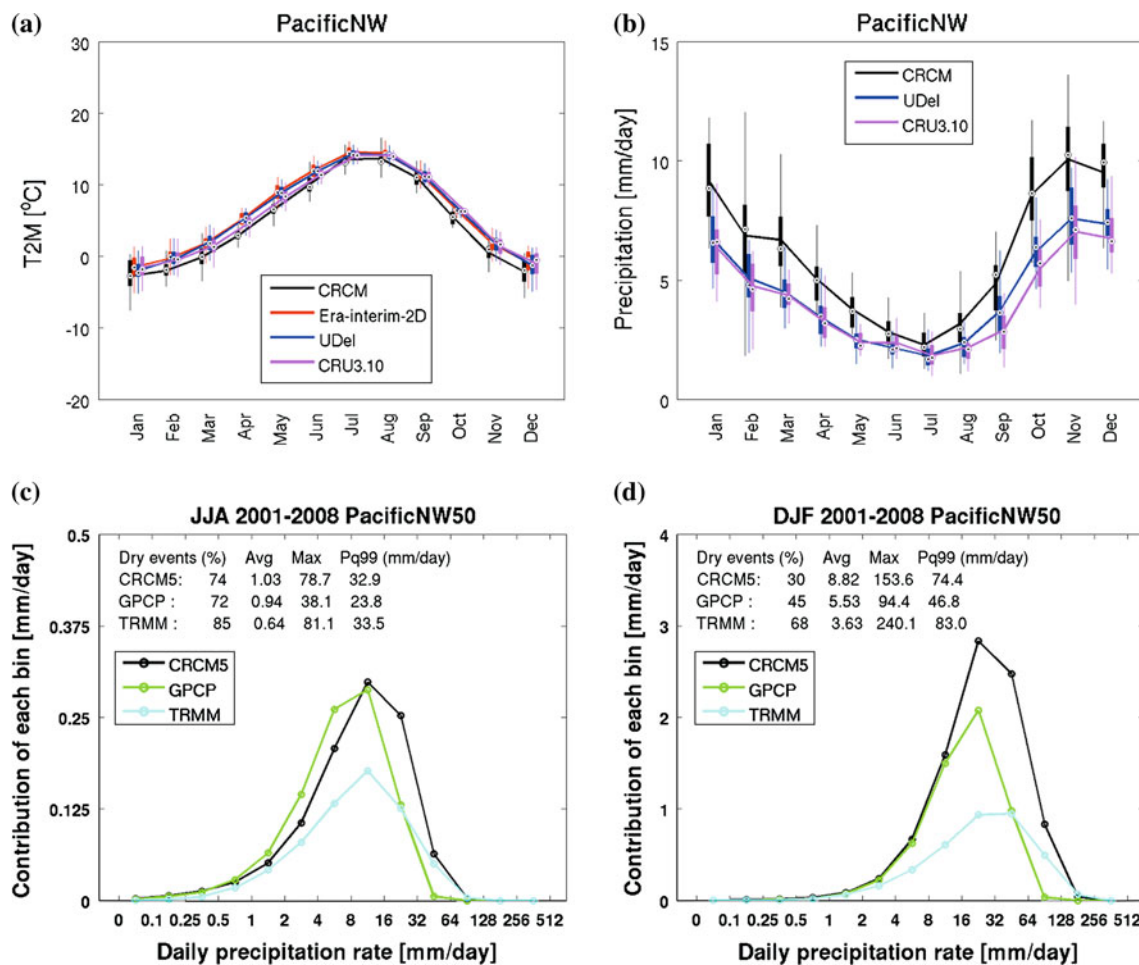


Fig. 15 Same as Fig. 10, but for the Pacific NW subdomain

there is substantial difference between simulation data and the observation-based datasets. Dry events are very frequent, 87–94 %, and low precipitation events prevail; on the other hand, the CRCM5 model produces a larger number of higher precipitation events. It is possible, however, that the observation datasets are prone to biases in such extremely dry conditions. In winter (Fig. 16d) the shapes of the precipitation frequency distributions are similar. The average daily precipitation amounts are however quite different: CRCM5 overestimates the average daily precipitation in comparison with observation datasets, which also differ between themselves.

The Desert subregion regroups Bukovsky’s South West and Mezquital basic subregions. As the region name suggests, it is covering mostly the regions with predominant arid desert (BWh, BWk) and steppe (BSh, BSk) Köppen climate types. Indeed, Fig. 17 demonstrates hot and mostly arid climate, with notable summer precipitation maximum, evidencing the presence of the NAM. There is a relatively important negative bias of simulated 2-m air temperature, which is present during the whole annual cycle. This cold

bias is also evident in Fig. 3. On the other hand, the annual precipitation cycle is remarkably well reproduced by the model simulation. The interannual variability is relatively small in temperature data, but is very strong in precipitation, in particular during the monsoon season, reflecting high variability of NAM, which will be addressed in more details in Sect. 5. In summer (Fig. 17c) the CRCM5 precipitation distribution is closer to that of TRMM, while in winter (Fig. 17d) both average daily precipitation and distribution demonstrate excellent coincidence with GPCP-1dd data.

4.3 Summer diurnal cycle in subregions

For the regions located to the South of 50°N, where TRMM data are available, and for the corresponding parts of Central, Pacific NW and Mt. West subregions, multi-annual (2001–2008) summer (JJA) mean diurnal precipitation cycles are shown in Fig. 18. CRCM5 hourly precipitation data are compared with the 3-hourly values from the TRMM dataset.

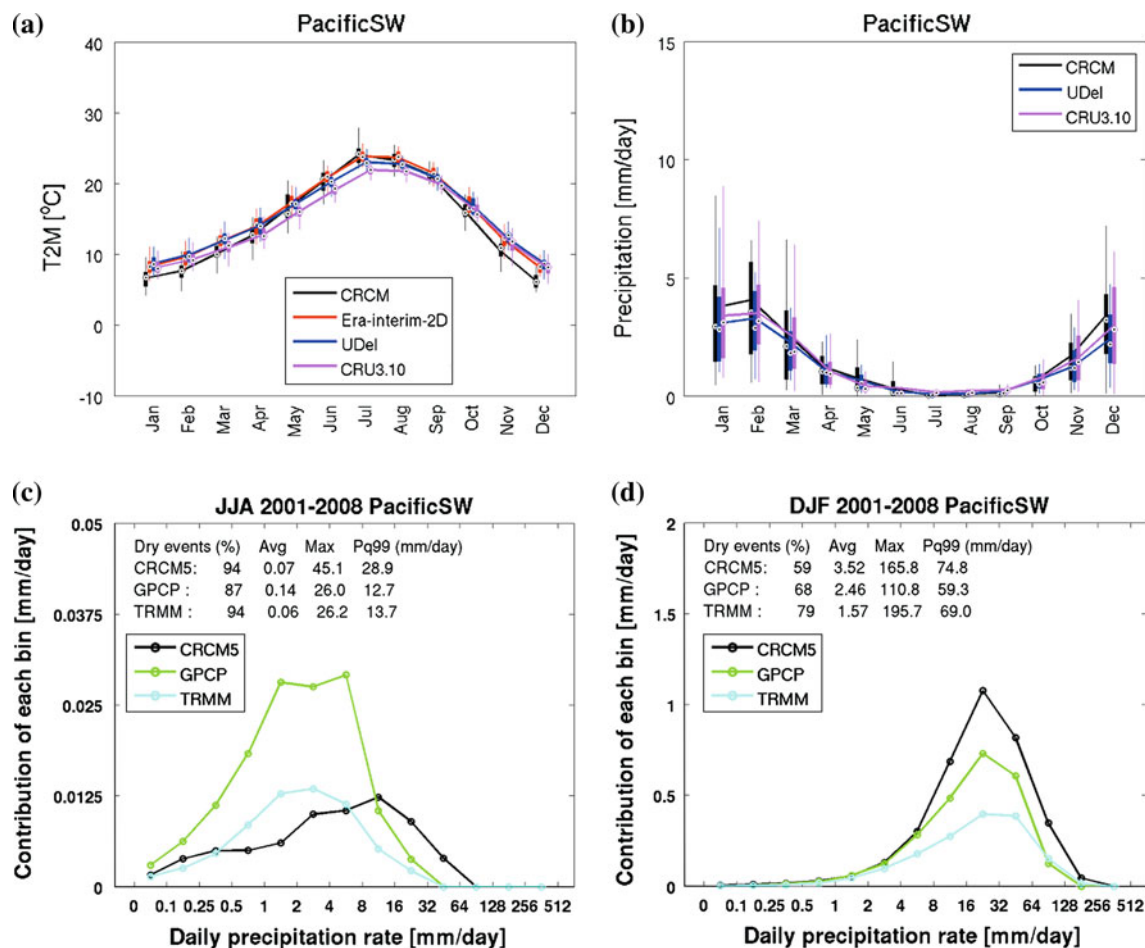


Fig. 16 Same as Fig. 10, but for the Pacific SW subdomain

In the Central subregion (Fig. 18a) a strong night-time precipitation maximum is present in TRMM data at around 6 GMT, which roughly corresponds to the local midnight. This precipitation maximum is not reproduced by the model. The rest of the diurnal precipitation cycle is well reproduced by the model, including the pronounced minimum at around 18GMT (local midday) and the late afternoon convective precipitation maximum. The nightly precipitation maximum in TRMM is related to the influence of the GPLLJ, which will be discussed in more details in Sect. 6.

In the vicinity of Great Lakes (Fig. 18b) the shape of the diurnal cycle, including nightly precipitation maximum, morning/midday minimum and afternoon rise is well reproduced by the model; however the absolute intensity of precipitation is underestimated by CRCM5 in comparison with TRMM.

In the East subdomain (Fig. 18c) the TRMM diurnal precipitation cycle has a pronounced nightly minimum, which is absent in the CRCM5 data. The daytime part of

the diurnal cycle (18–24 GMT) is well reproduced by the model.

Similar TRMM diurnal cycle shape is present in the South subdomain (Fig. 18c) and in the Mt. West subdomain (Fig. 18e). However, in these subregions the CRCM5 model is able to reproduce both the timing of nightly precipitation minimum and the daytime part of the cycle.

The diurnal cycle of the northern part of the Pacific NW subregion (Fig. 18f) is predominantly flat according to both TRMM and to CRCM5. The CRCM5 data contain a broad maximum in the morning hours, characteristic the diurnal cycle of precipitation over the oceans (Tian et al. 2005).

In the Pacific SW subregion (Fig. 18g) the simulated and observation-based diurnal cycles are generally similar: the night-time minimum and afternoon maximum are present on both curves. The structure of CRCM5-simulated daily cycle is more complex, with additional maximum at 15 GMT (~ 7 LST), early in the morning, which as in the case of Pacific NW might testify the influence of the Pacific Ocean.

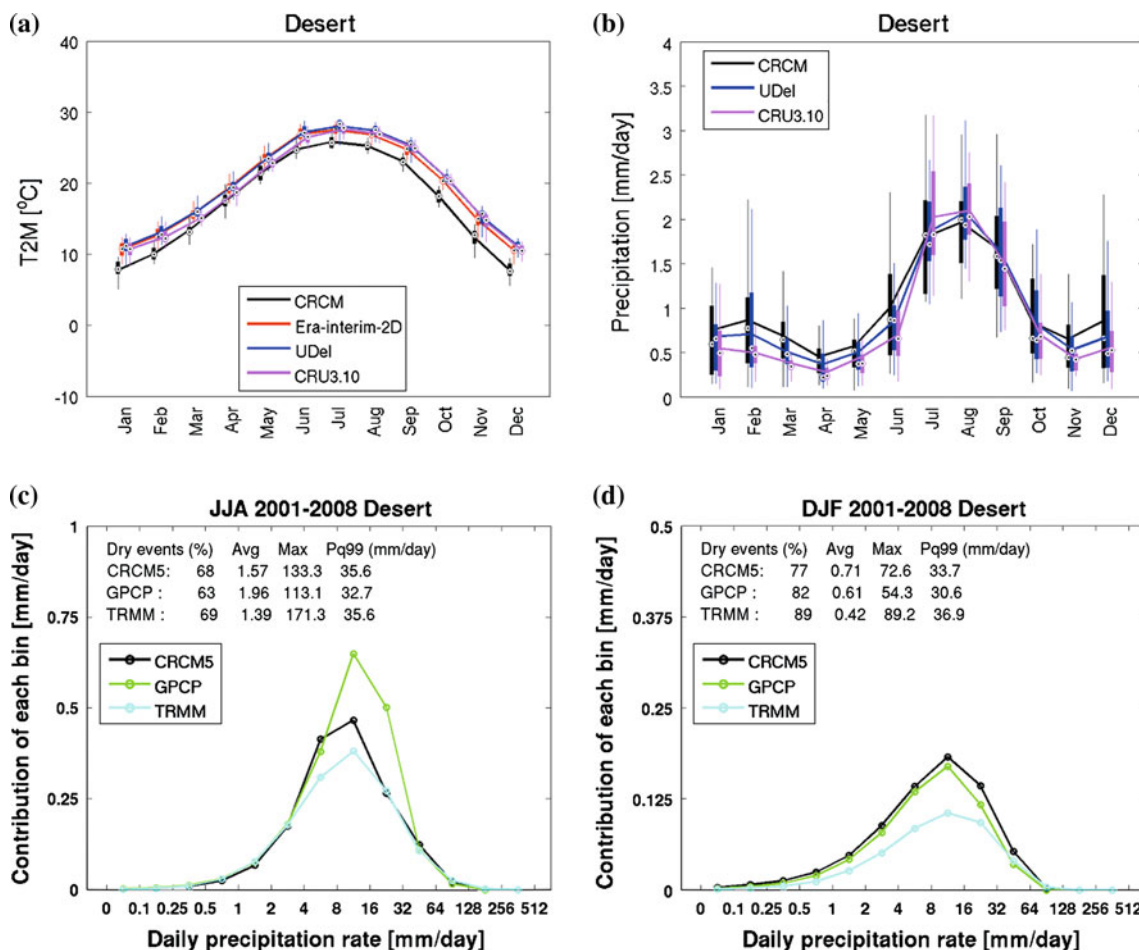


Fig. 17 Same as Fig. 10, but for the Desert subdomain

In the Desert subregion (Fig. 18h) the simulated and observation-based diurnal cycles almost coincide, with the simulated afternoon maximum stronger and occurring slightly earlier than according to the TRMM data.

In general, we can conclude that the CRCM5 model is able to reproduce adequately the thermally-driven atmospheric convection, responsible for the afternoon rise of precipitation. The processes responsible for the night-time precipitation peculiarities are not yet reproduced entirely satisfactorily by the model.

5 Comparison with other RCMs

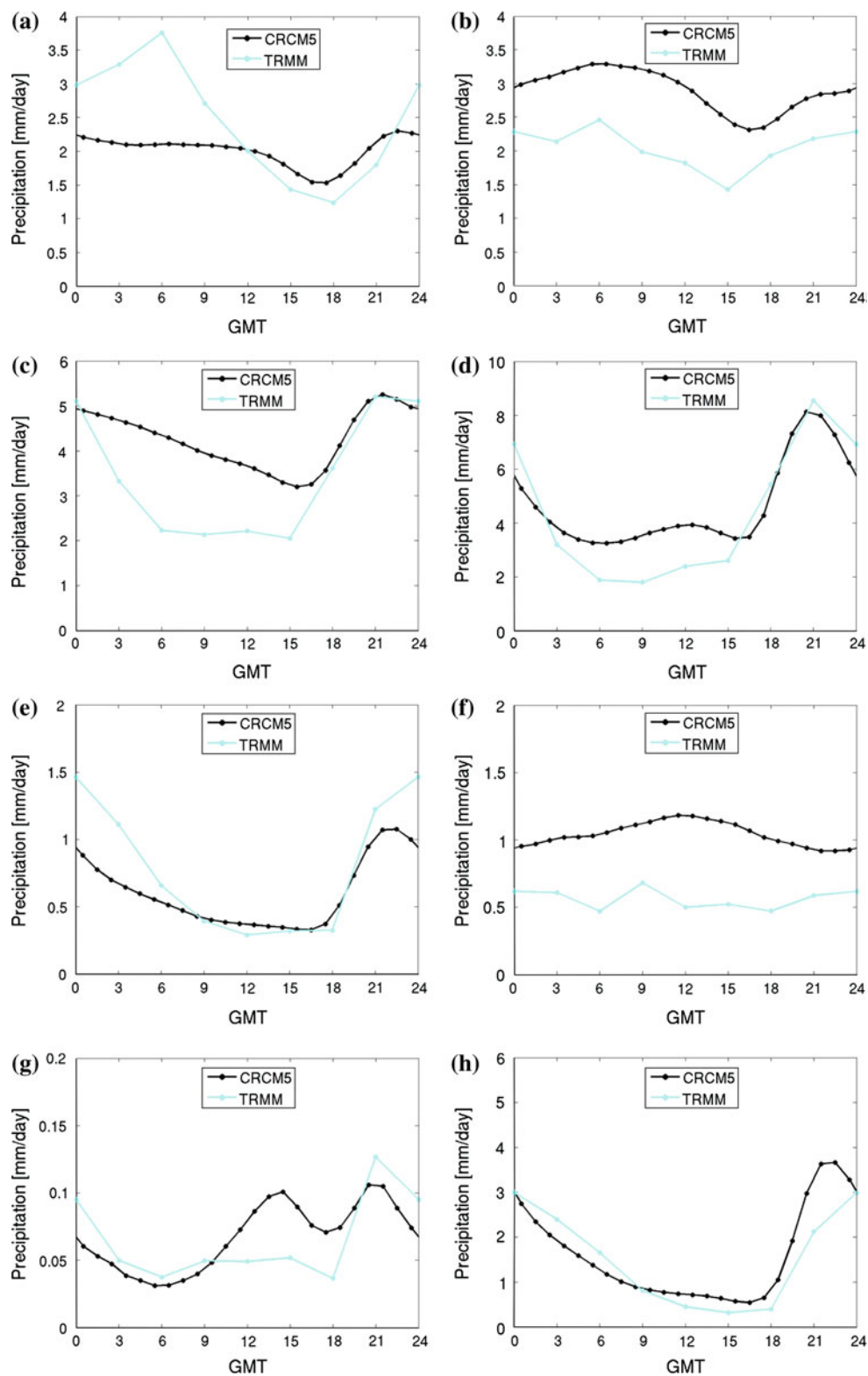
5.1 Comparison with previous versions of CRCM

As mentioned in the Introduction, the 5th generation CRCM is considerably different from previous versions 3 and 4 so that these models can be considered as independent. It is important to estimate the effectiveness of such a radical change by comparing the performance of CRCM5

with that of previous versions of CRCM and to position its performance against earlier achievements. It is important to mention however that the simulation periods, simulation domains, forcing and reference datasets, diagnostic subdomains, seasons and approaches to data analysis differ substantially in published data, making the direct comparison of simulated climatology difficult. A qualitative analysis, based on figures and text of publications, is the remaining option. We can also confront roughly similar quantitative values, obtained in closest possible conditions, but such a comparison can only be considered as an approximate estimation.

Strong temperature and precipitation biases were present in the NCEP/NCAR reanalysis-driven CRCM3 simulations presented by Plummer et al. (2006). In particular, a strong wintertime warm bias (up to +10 °C) was present over the snow-covered northern regions of the continent, while cold bias (up to -7 °C) prevailed over the southern part of the simulation domain. This cold bias subsisted in summertime, extending to most part of Rocky Mountains, while the bias over the rest of the continent was around +2 °C. In the

Fig. 18 Summer (JJA) diurnal precipitation cycle for the 2001–2008 period, CRCM5 (black) and TRMM (blue). Subdomains: **a** Central, **b** Great Lakes, **c** East, **d** South, **e** Mt. West, **f** Pacific NW, **g** Pacific SW, **h** Desert



CRCM5 simulation presented in this article, the former winter warm bias, caused primarily by imperfections in the treatment of snow in the land-surface scheme, has practically disappeared. The CRCM5 still exhibits a cold bias in

southern and mountainous regions, albeit it is weaker than in CRCM3 simulations. The precipitation was strongly overestimated in the CRCM3 simulations: a wet bias of 1–3 mm/day obtained in summer over most of the

continent and in winter over western North America. Similar characteristics of the CRCM3-simulated precipitation were presented in Jiao and Caya (2006), where reasons of this underperformance were analysed and possible solutions proposed. Compared with CRCM3 results, the performance of CRCM5 in simulating the precipitation, as described in Sect. 3, has been dramatically improved. The multi-annual averaged precipitation rate is well reproduced by the model over the most part of the North American continent. It is still overestimated in problematic coastal regions, most notably the Pacific NW.

In Brochu and Laprise (2007) the annual-average values of precipitation rate and 2-m air temperature for the period 1987–1994 as simulated by CRCM3 and a development version of CRCM4, driven by NCEP/NCAR reanalyses, were shown for the Mississippi river basin, which can be approximately related with Central and South Bukovsky subdomains. The average bias from the reference dataset ensemble is 1.1 mm/day for CRCM3 and 0.2 mm/day for CRCM4. The average bias for the 1989–2008 CRCM5 data are 0.3 mm/day and 0.2 mm/day for the Central and South subdomains, respectively. The 2-m temperature biases were 0.55 °C for CRCM3 and 0.95 °C for CRCM4. In the CRCM5 simulations for 1989–2008, the corresponding biases are –1.1 °C for Central and –0.7 °C for South subdomain. Thus, the performance of the CRCM5 model is in general comparable with that of CRCM4 for the annual mean.

Paquin et al. (2009) reported upon CRCM4 simulations driven by ERA-40 for 1961–2000. They noted CRCM4 precipitation biases in JJA ranging from –0.5 to –2 mm/day in the Mississippi and Deep South area, while CRCM5 now exhibits biases of –0.3 mm/day and +0.4 mm/day for the Central and South subdomains, respectively. For DJF, CRCM4 precipitation biases ranged from –1.5 to –2.5 mm/day in the Deep South and East Coast areas, where CRCM5 now exhibits biases of +0.1 (South subdomain) and +0.7 mm/day (East subdomain), correspondingly. Over the Rocky Mountains in DJF, CRCM4 simulations had a precipitation bias of 1.5–5 mm/day while CRCM5 now has in corresponding subdomains a bias of 0.6 mm/day (Mt. West subdomain) to 2.3 mm/day (Pacific NW subdomain). CRCM4 temperature biases in DJF ranged from –4 to –7 °C over the Rocky Mountains where CRCM5 bias is of the order of –1.2 (Mt. West) to –2.6 °C (Pacific NW). Hence in terms of seasonal mean statistics, CRCM5 outperforms CRCM4.

5.2 Comparison with other RCMs

The performance of CRCM5 simulation can also be compared with that of other RCMs. While no publications using Bukovsky regions yet exist, similar analysis for other subdomains and simulation periods have been done. In

Bukovsky and Karoly (2011), the NCEP/NCAR reanalysis-driven WRF RCM has been used for simulating the 1990–1999 period. Differences between simulated data and those of NARR and NCEP/NCAR reanalyses are listed for the MJJA season for the Continental US zone (Bukovsky and Karoly 2011, Fig. 2d), roughly corresponding to the Bukovsky Central zone. The maximum 2-m air temperature bias for this region equals to –3.96 °C, while the JJA bias in CRCM5 simulation equals to 0.8 °C. For precipitation, the bias of 1.43 mm/day is indicated by Bukovsky and Karoly (2011), and the JJA bias in CRCM5 simulation equals to –0.3 mm/day. Maximum biases for all domains and datasets in Bukovsky and Karoly (2011) are –3.61 °C and –1.16 mm/day, while maximum biases for CRCM5 are –1.9 °C and 0.7 mm/day, correspondingly.

The CRCM5 performance can also be assessed by comparison with preliminary NARCCAP project results presented in Mearns (2010) and published in Mearns et al. (2012) for NCEP reanalysis-driven RCM simulations over the 1980–2004 period. Again, a direct quantitative comparison is impossible because of differences in simulation configurations and different diagnostic subdomains. Approximate comparison can still be useful. For two domains, the California Coast and Deep South, Mearns (2010) presented the interannual correlation coefficients for annually averaged precipitation between six participating RCMs, their ensemble mean and observation-based reference dataset ensemble mean. The California Coast domain is close to the Bukovsky Pacific SW subregion and the Deep South domain can be related to the Bukovsky South subregion. For the California Coast, the ensemble correlation coefficient, 0.95, is higher than that for most ensemble members, except CRCM4 that equals it. The corresponding CRCM5 Pacific SW correlation coefficient is also 0.95. For the Deep South, the RCM ensemble correlation coefficient is 0.65; only two participating models have slightly higher correlation coefficient, CRCM4 being one of them. For the Bukovsky South region, the CRCM5 correlation coefficient equals to 0.62. In Mearns et al. (2012) the precipitation and 2-m temperature correlation statistics were presented for four subregions, including Southern California (close to Bukovsky's Pacific NW), Great Plains (“Central”), South-Central US (“South”) and Atlantic Coast (“East”). The CRCM5 values are close to the best values shown by NARCCAP-participating models, and equal or surpass the ensemble-mean values both for precipitation and 2-m temperature, with the exception of temperature in the Pacific SW subregion. The visual comparison of annual temperature and precipitation cycles for those regions, shown in Figs. 10, 12, 13 and 16, with those shown in Figure 11 of Mearns et al. (2012) shows that the CRCM5 biases from observed values are comparable with those of NARCCAP models.

It can thus be concluded that the performance of CRCM5 in terms of interannual anomaly correlation coefficient is comparable to that of spectrally-nudged CRCM4 and of other modern RCMs.

6 North American Monsoon

As it has been shown in Sect. 4.2, the NAM is very important for the arid areas of Southwestern North America. The monsoon provides most of the annual precipitation over this large region (Fig. 17b).

The NAM zone can be well seen in Figs. 4a and 5a, where the CRCM5-simulated summer precipitation data are shown. A relatively narrow precipitation band is formed along the Pacific Coast of Mexico and the Gulf of California region. The northern limit of intense precipitation area reaches the New Mexico and Arizona states. In comparison with observation-based datasets, a relatively weak dry bias (<2 mm/day) can be noted in comparison with CRU TS3.1 data (Fig. 4b); the bias is lower, if CRCM5 data are compared with UDel dataset, as shown in Fig. 4c. The relative difference figures show that this dry bias is of order of 100 % of precipitation rate and occurs over a large domain, covering most part of the Southwestern USA and of the Northwestern Mexico (Fig. 4d). The area of strong relative dry bias from UDel data is smaller (Fig. 4e).

In order to better assess the performance of CRCM5 in simulating NAM and compare simulation results with observations, two small subdomains, located in the NAM area, are studied: the CORE subdomain, covering parts of Baja California peninsula and Gulf of California coast, and the AZNM subdomain, covering parts of Arizona and New Mexico states (Gutzler et al. 2009). The CORE subdomain is located in the centre of NAM-influenced area, while the AZNM subdomain is at its northern limit. The simulation grid points, corresponding to these subdomains, are presented in Fig. 19. As in the Sect. 4, annual 2-m temperature and precipitation cycles will be presented, along with seasonal and diurnal precipitation distributions.

The temperature and precipitation patterns for the CORE zone are presented in Fig. 20. The summer, autumn and winter 2-m air temperature is simulated by CRCM5 with a notable cold bias of $\sim 3\text{--}5$ °C. This cold bias was clearly distinguishable in Fig. 3b–d, both in summer and in winter months. The smallest bias is present in spring, when it is comparable with the discrepancy between the reference datasets ($2\text{--}3$ °C during the whole annual cycle).

The shape of the precipitation annual cycle with two precipitation maxima is well reproduced by the model. The strongest precipitation maximum, associated with NAM, closely reproduces the observation-based datasets with the

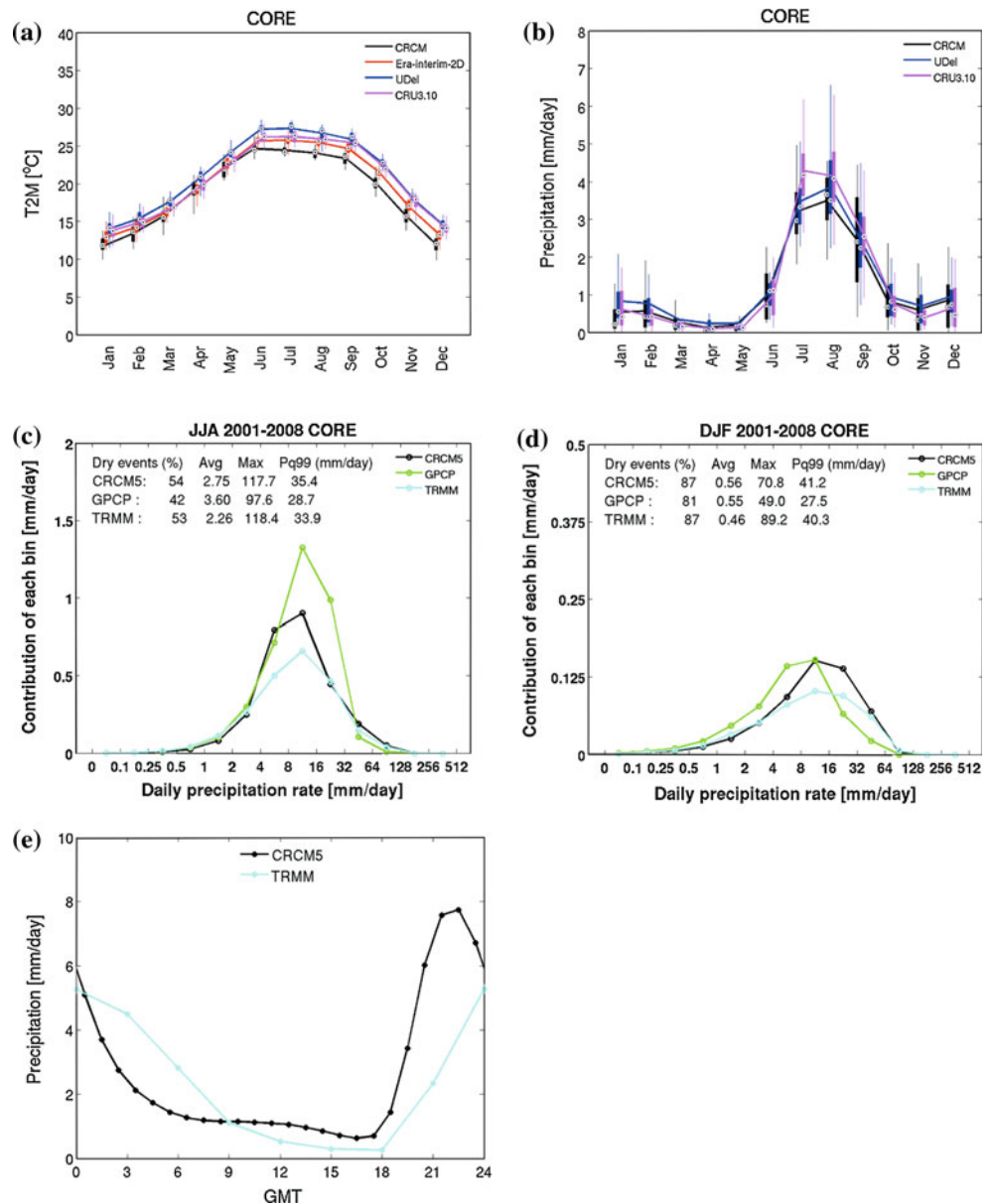


Fig. 19 The map of subregions in the North American Monsoon zone: AZNM and CORE subregions (Gutzler et al. 2009). Actual simulation grid tiles within these subregions are presented

correct timing. The maximum simulated precipitation in July–August however is slightly weaker than in UDel and substantially weaker than that in the CRU TS3.1 data. Note the substantial difference between these two observation datasets during this period. According to Fig. 5b and to the average JJA 1998–2008 precipitation levels shown in Fig. 20c the GPCP-1dd precipitation values are even higher for this region than those of UDel and CRU TS3.1. Figure 20b demonstrates a large interannual variability of monthly mean precipitation values, both in simulation and in observation datasets; it is especially high during the NAM season. In summer the CRCM5 precipitation distribution is close to the observation datasets, but the average daily precipitation lies between TRMM and GPCP-1dd values (Fig. 20c). In wintertime (Fig. 20d) the precipitation frequency distributions of GPCP-1dd and TRMM are notably different. CRCM5 produces more higher-rate events than both reference datasets. The precipitation cycle of simulation data in summer, during NAM, exaggerates the afternoon precipitation maximum (0 GMT, or ~ 16 LST), which occurs too early (21–22 GMT, $\sim 13\text{--}14$ LST), and is much more intense and of shorter duration than in TRMM (Fig. 20d).

In the AZNM zone (Fig. 21) the 2-m air temperature is also reproduced with a notable cold bias, especially in wintertime. The shape of the precipitation annual cycle is in general well reproduced by the model, although the average NAM-related summer precipitation maximum is much smaller (by ~ 0.5 mm/day, or ~ 50 % of the CRCM5 value) than in observation-based datasets. The simulated winter precipitation maximum is notably higher

Fig. 20 Same as Fig. 10, but for the CORE subdomain; the panel e shows the summer (JJA) diurnal precipitation cycle for the 2001–2008 period, CRCM5 (black) and TRMM (blue)



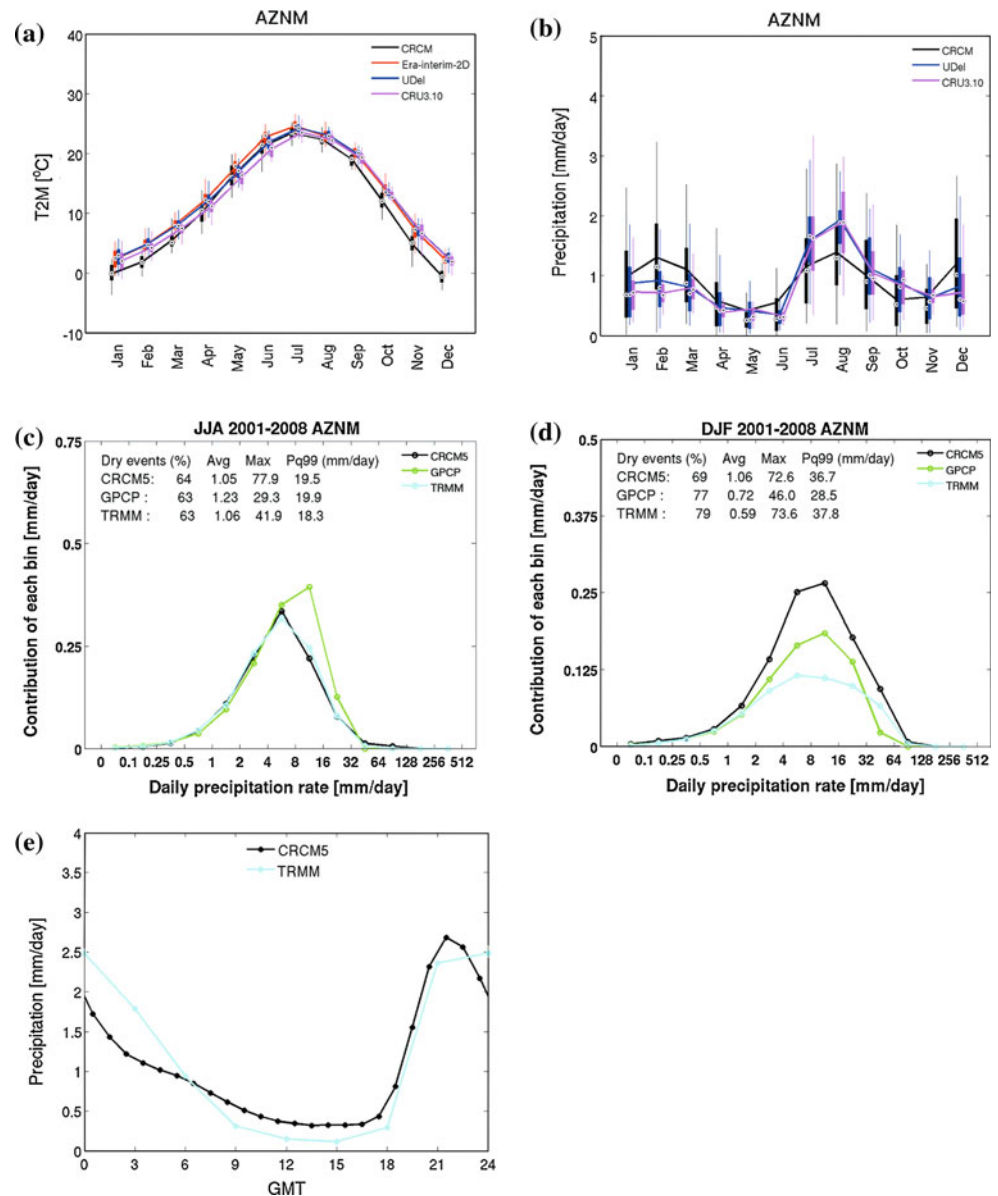
than that in the CRU TS3.1 and UDel data. As in the CORE region, the precipitation frequency distributions of these reference datasets differ among themselves, both in summer and in wintertime. The simulated precipitation frequency distribution is very close to that of TRMM in summer (Fig. 21c), during the NAM season. In winter the CRCM5 distribution shape is similar to those of reference datasets, but the average precipitation amount is higher (Fig. 21d). The summer precipitation cycle is in general reproduced by the model (Fig. 21e), but as in the CORE zone, the simulated afternoon precipitation maximum is shifted from 0 GMT (~16 LST) towards 22 GMT (~14 LST) and is of shorter duration than in the TRMM data.

In general, the ERA-Interim-driven CRCM5 model is capable of correctly simulating the annual cycle of the

monsoon and, in the southern part of the NAM region, it reproduces some important multi-annual average precipitation characteristics (frequency, distribution and intensity), while the precipitation intensity is underestimated in the northern part of the NAM area (New Mexico and Arizona states, in particular). The interannual variability of simulated NAM-related precipitation is very high and is comparable with that of observation-based reference datasets.

The large interannual variability of NAM reflects its strong dependence on important climatic factors, such as multi-annual oscillation processes in the climate system. The influence of interannual variations in the intertropical convergence zone in the eastern tropical Pacific to NAM has been established by Hu and Feng (2002), and the role

Fig. 21 Same as Fig. 20, but for the AZNM subdomain



of Madden-Julian oscillation and of easterly equatorial waves has been studied by Lin et al. (2008). It is important to mention that the geographical location of these processes is well beyond the North American regional simulation domain. Castro et al. (2007) have shown that the quality of NAM simulation by RCMs is strongly dependent on external driving data that have to reproduce correctly the essential teleconnections and climatology. The degree to which the SST is reproduced in the area, adjacent to the NAM zone, is also of primary importance: it has been shown by Mitchell et al. (2002) that the NAM, especially over its northern area in Arizona, strongly depends on the SST in the northern part of the Gulf of California. While the ERA-Interim SST data, used in these CRCM5 simulations, are based on observations, it can be supposed that

relatively small biases in SST can still be present in these data and contribute to the NAM-associated precipitation bias in the northern part of the NAM area. More detailed study is required to determine the relative influence of different factors to the performance of the CRCM5 model in the NAM area.

7 Great Plains Low-Level Jet

The GPLLJ is easily distinguishable on maps of averaged (JJA 1998–2008) horizontal wind at 925 hPa, presented in Fig. 22. The band of strong southerly winds, blowing along the eastern slope of Rocky Mountains, simulated by CRCM5 model, (Fig. 22a) is very similar to that of ERA-

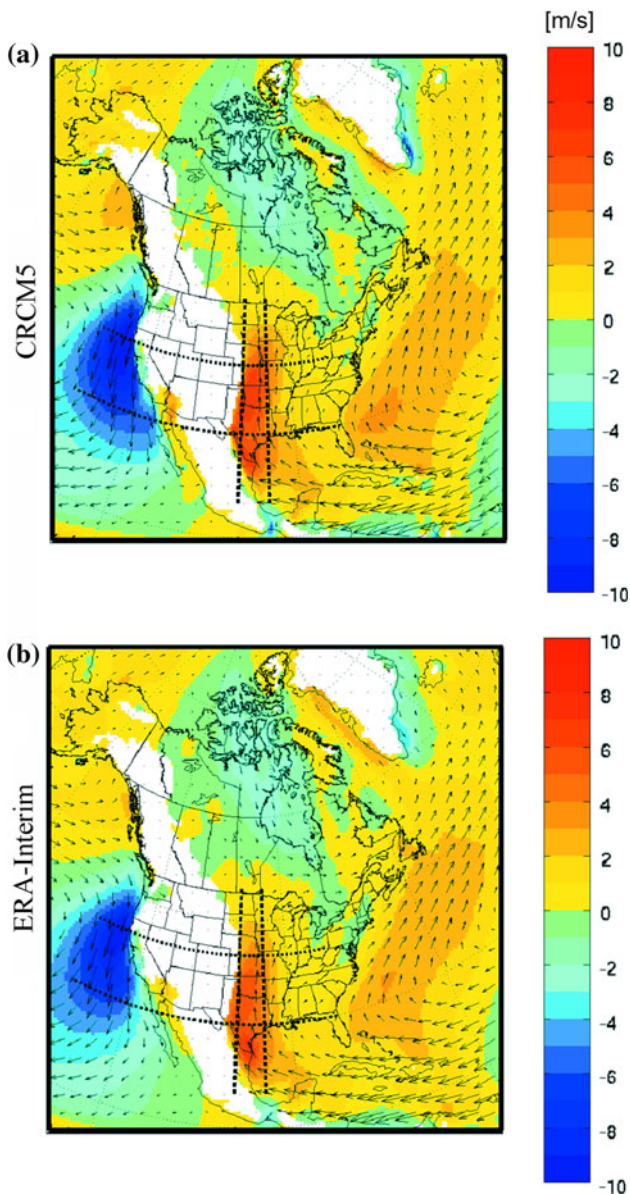


Fig. 22 Mean JJA meridional (in color) and total horizontal (arrows) winds (m/s) at 925 hPa, for the 1998–2008 period, for **a** CRCM5 simulation and **b** ERA-Interim reanalysis. The intersection of the zonal (30°N–40°N) and meridional (95°W–100°W) bands (black dotted lines) define the GPLLJ domain

Interim (Fig. 22b). The area of strong winds extends between approximately 25°N and 45°N. Two parts can be distinguished: the northern one, roughly between 30°N and 45°N, and the southern one, in the area of lower elevations, between 25°N and 30°N, over the Texas coastal plains and Gulf of Mexico. The southern part corresponds to the area where the easterly winds, associated with the Caribbean Low-Level Jet (CALLJ; Amador 1998) that brings moisture from the Caribbean Sea and the Gulf of Mexico, meet the mountainous continental coast, turn northward and form the GPLLJ (Mo et al. 2005). This transition of

easterly to southerly winds is clearly seen in ERA-Interim (Fig. 22b) and is well reproduced by CRCM5 (Fig. 22a).

In order to assess in details the ability of CRCM5 in reproducing the structure and diurnal evolution of the GPLLJ, meridional and zonal cross-sections of GPLLJ winds will be studied. The region defined by the intersection of the zonal and meridional bands shown in Fig. 22, i.e. the region delimited by 95°W–100°W and 30°N–40°N, experience the strongest winds and corresponds to the region studied by Jiang et al. (2007).

Figure 23 presents a meridional cross-section of meridional winds, zonally-averaged in the band between 95°W and 100°W, for 0, 6, 12 and 18 GMT, both for the CRCM5 simulation and the ERA-Interim reanalysis. In ERA-Interim the area of strong winds extends from approximately 25°N to 45°N. The diurnal cycle of the GPLLJ is quite pronounced between 30°N and 40°N. The jet reaches its maximum strength and meridional extent at around 6 GMT (local solar midnight) and the southerly winds are then concentrated in a shallow layer near the surface; the strongest winds are located at around 37°N. The wind force diminishes towards 12 GMT (6 LST). At 18 GMT (12 LST) it reaches its minimum strength and meridional extent, and the vertical extent of the jet zone is then at its highest. At 0 GMT (18 LST) the GPLLJ begins strengthening and decreases its vertical extent. A return northerly flow in the upper troposphere is present above the GPLLJ and it exhibits a diurnal cycle synchronised with that of the GPLLJ.

The general structure and diurnal cycle of the CRCM5-simulated GPLLJ and return flow are close to that in the ERA-Interim reanalysis. The simulated jet is slightly shifted to the north, with a “core” located at around 37°N persisting at all times. The simulated GPLLJ at 6 GMT is slightly deeper than in ERA-Interim.

Figure 24 presents a zonal cross-section of meridional winds, averaged in the latitude band between 30°N and 40°N for the same time slices, as well as the underlying topography. It can be clearly seen that the GPLLJ is located near the eastern slope of the Rocky Mountains. The diurnal cycle of the GPLLJ is also clear in this figure, with the maximum jet strength at 6 GMT and the minimum at 18 GMT. The evolution of the depth of the jet zone confirms that described earlier in the zonal cross-section. Noteworthy is the return northerly flow in the upper troposphere, which is located somewhat to the east of the GPLLJ (Fig. 24), and exhibits fluctuations in its depth as well as its intensity. The general structure and diurnal cycle of CRCM5-simulated meridional winds in the cross-section are very close to that in the ERA-Interim reanalysis.

Figure 25a shows the diurnal evolution of the meridional winds averaged over the GPLLJ zone shown as a dashed square in Fig. 24, between 700 and 1,000 hPa. The

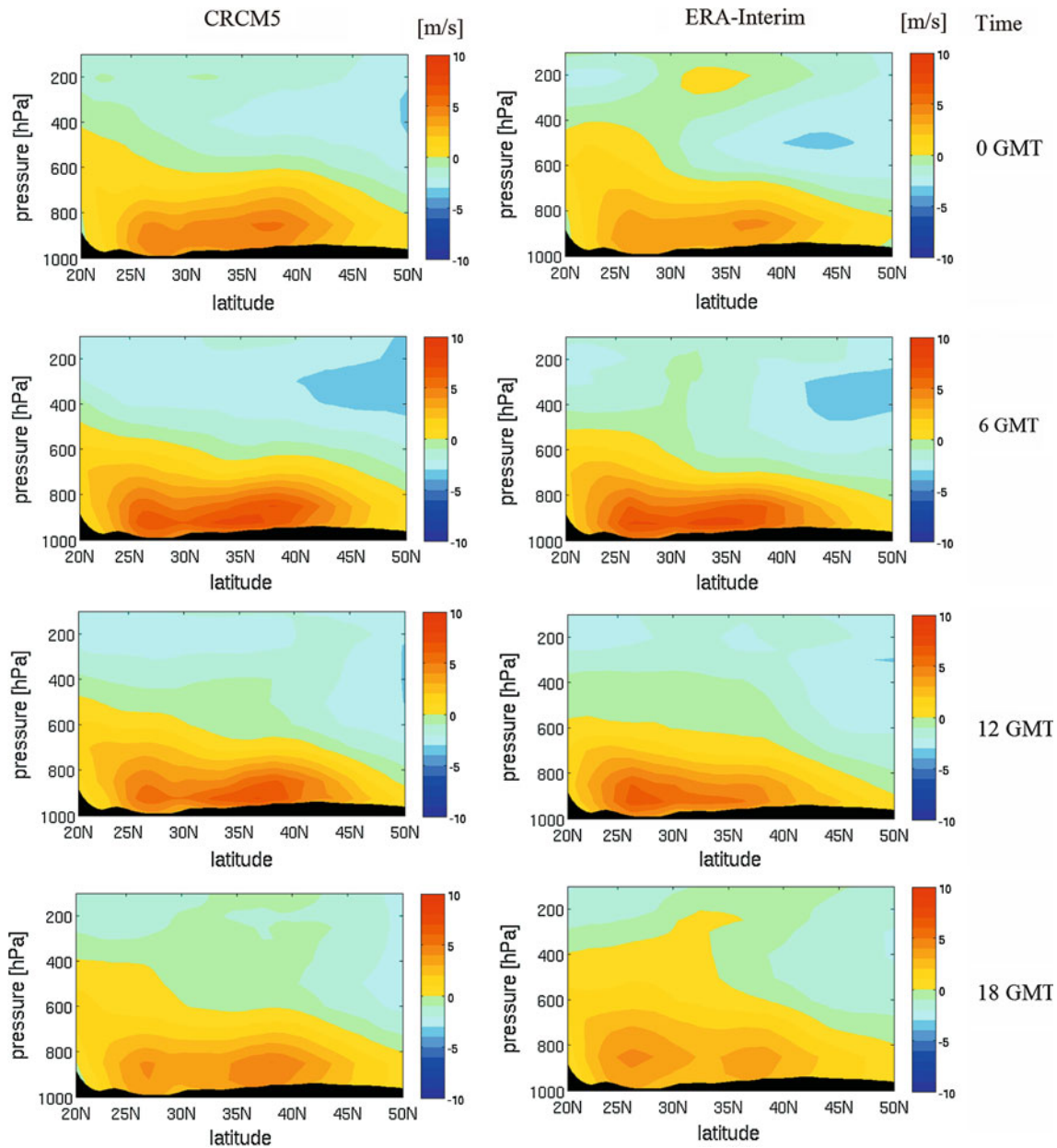


Fig. 23 Meridional cross-section of the mean JJA meridional wind (m/s), zonally averaged between 95°W and 100°W , for the 1998–2008 period, for CRCM5 simulation (left panels) and ERA-

Interim (right panels), at 0, 6, 12 and 18 GMT (top to bottom). The zonally averaged orography profile is outlined in black

previously described diurnal cycle is evident here: the simulated winds reproduce the diurnal cycle of the ERA-Interim winds, but the magnitude of winds is slightly overestimated. The diurnal evolution of wind magnitude and of the vertical structure of jet winds correspond well to that in the NCEP regional reanalysis (Mo et al. 2005) and to wind profiler observations (Higgins et al. 1997).

The moisture brought by the jet from the Gulf of Mexico is responsible for summer precipitation in the GPLLJ zone. The annual cycle of precipitation in this region is shown in Fig. 25b. The interannual variability of the precipitation cycle

is strong, (2–4 mm/day), compared with average monthly precipitation rates. The annual maximum of simulated precipitation is shifted from May–June for observation data to March–May. The diurnal cycle of summer precipitation over the GPLLJ region is shown in Fig. 24c–f for the CRCM5 simulation and the TRMM data. The diurnal cycle is rather peculiar for a mid-latitude region where normally night-time minimum and afternoon maximum occur (e.g., Fig. 18c for the East subdomain, Fig. 25c for the southern part of the GPLLJ zone, $30\text{--}35^{\circ}\text{N}$). Instead, in the GPLLJ region to the north of 35°N , the precipitation cycle is more typical of

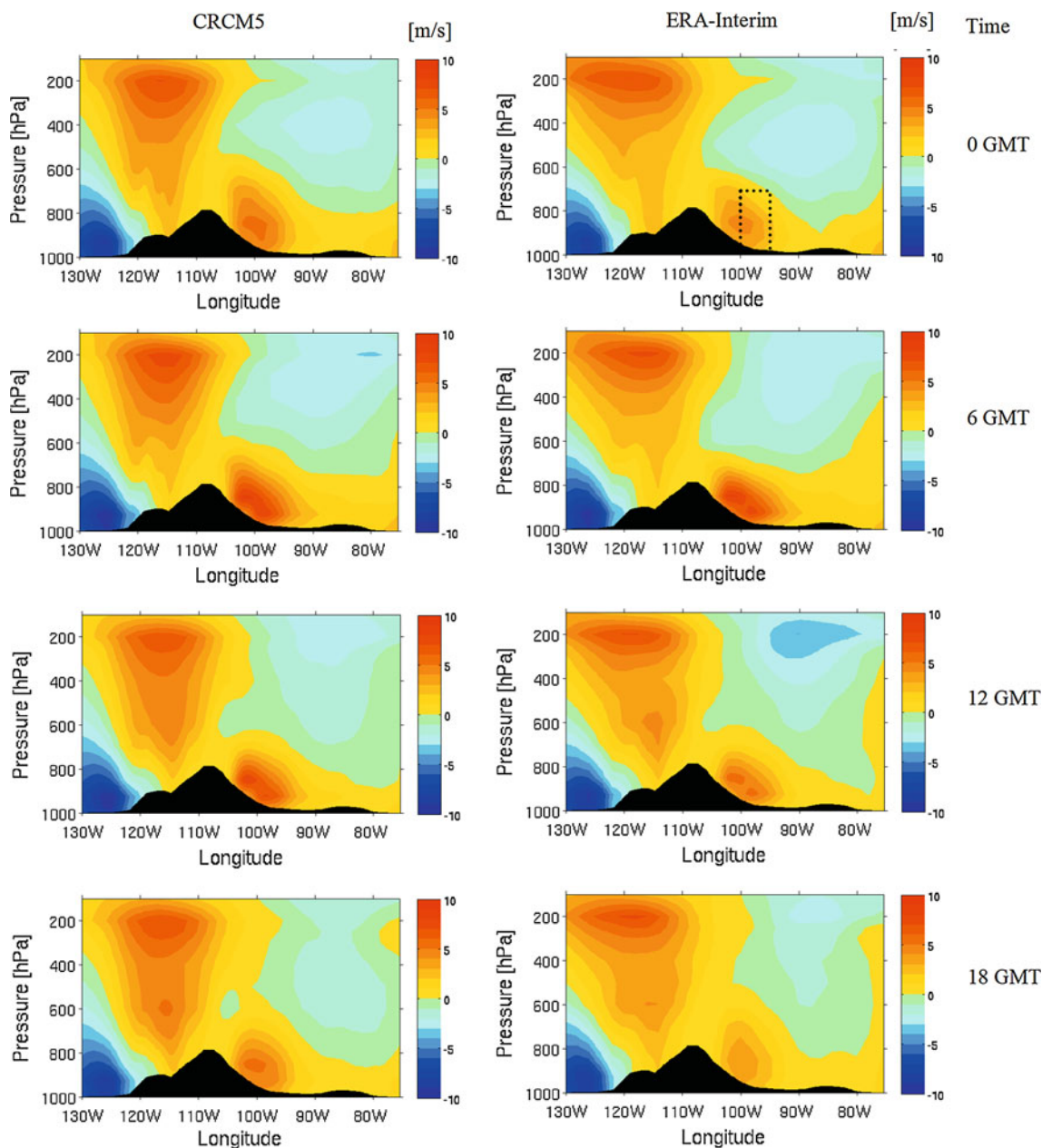


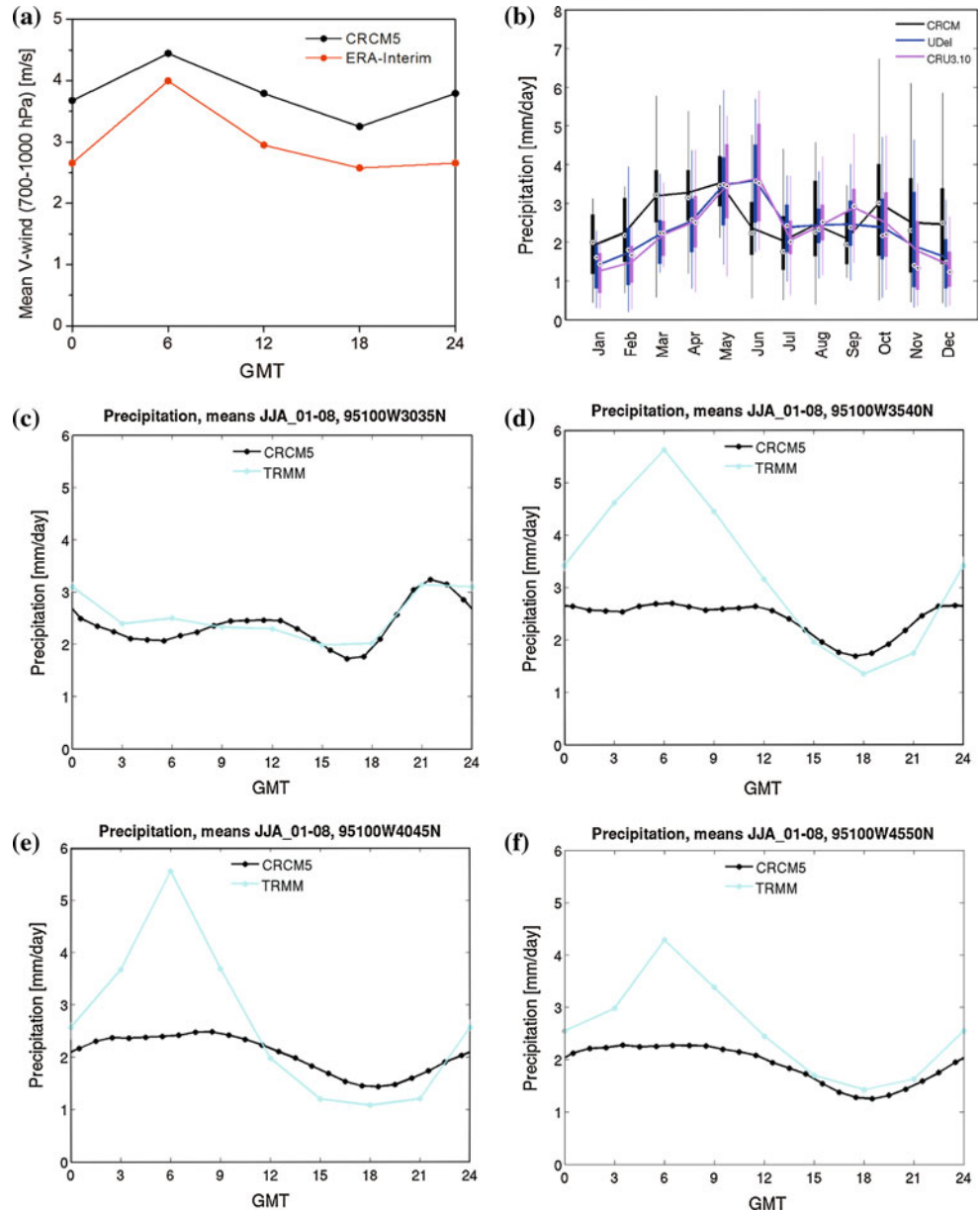
Fig. 24 Zonal cross-section of the mean JJA meridional wind (m/s), meridionally averaged between 30°N and 40°N, for the 1998–2008 period, for CRCM5 simulation (left panels) and ERA-Interim (right panels), at 0, 6, 12 and 18 GMT (top to bottom). The meridionally

averaged orography profile is outlined in black. The dotted square in the top right panel corresponds to the cross-section that is used for the analysis presented in Fig. 25a

tropical regions with a maximum at night-time, centred on 6 GMT (0 LST), according to the TRMM dataset (Fig. 25d–f). Note that the night-time precipitation maximum zone (35–50°N) is shifted northwards from the strongest GPLLJ wind zone (30–40°N). This location of night-time precipitation maximum zone is in accordance with the satellite-based data of Tian et al. (2005). In this zone the precipitation maximum can be related with the night-time enhancement of the GPLLJ, occurring a couple of hours earlier (local midnight, according to Fig. 25a). Note however that the temporal

resolutions of the ERA-Interim data (6 h) and the TRMM data (3 h) limit the possibility of making definite conclusions on processes of comparable and shorter characteristic time. While the CRCM5 simulation reproduces well the diurnal cycle of the GPLLJ, it can be seen in Fig. 25d–f that the peculiar structure of the diurnal cycle of precipitation is not reproduced adequately by the model. The night-time precipitation peak is present in the CRCM5 data in these figures, but is substantially lower than that of the TRMM data. A day-time precipitation minimum is present in both simulation and

Fig. 25 **a** Mean diurnal cycle of the JJA meridional wind, for the 1998–2008 period, for the cross-section shown in the *top right* panel of Fig. 24, for CRCM5 and ERA-Interim; **b** mean annual precipitation cycle, for the 1989–2008 period, for the GPLLJ domain. Mean JJA diurnal cycle of precipitation, for the 1998–2008 period, for CRCM5 and TRMM data for four $5^\circ \times 5^\circ$ zones are shown in the *middle* and *bottom* panels: **c** $95\text{--}100^\circ\text{W}$, $30\text{--}35^\circ\text{N}$, **d** $95\text{--}100^\circ\text{W}$, $35\text{--}40^\circ\text{N}$, **e** $95\text{--}100^\circ\text{W}$, $40\text{--}55^\circ\text{N}$, **f** $95\text{--}100^\circ\text{W}$, $45\text{--}50^\circ\text{N}$



TRMM data. The difficulties of reproducing the GPLLJ diurnal precipitation cycle have already been reported in previous studies (e.g., Lee et al. 2007). Planetary boundary layer scheme and deep convection parameterization imperfections have been proposed as possible causes. More detailed study of the CRCM5 performance in the GPLLJ area might be required for further improvement of the model.

8 Summary and conclusions

The performance of the CRCM5 simulations driven by ERA-Interim reanalysis over the North American CORDEX domain has been assessed in several different ways.

The continental-scale performance of the CRCM5 model has been compared with the reference observation-based datasets and the ERA-Interim reanalysis. The simulation exhibits a cold bias reaching $4\text{--}6^\circ\text{C}$ in the western part of the continent in summertime; this bias persists over Mexico during the whole annual cycle. However, the model has shown considerable skill in reproducing the precipitation patterns over most part of the continent. In comparison with CRU TS3.1 and UDel datasets, the non-compensated biases of ground-based observations between Canada and United States have been revealed. Mountainous and coastal regions remain problematic for the model, possibly because the horizontal resolution in the simulation is insufficient for such complex conditions.

More detailed analysis of air temperature and precipitation patterns has been performed for ten large and relatively climatologically homogenous subregions of the North American continent, with quantitative estimations of average values and biases summarised in Tables 2, 3, and 4. The simulated interannual correlations between seasonal precipitation and 2-m temperatures are close to those in the reference observation databases, with only few exceptions. It was shown that the shape of the annual cycle of 2-m air temperature and precipitation is in most cases generally well reproduced by the model as well as the interannual variability of these variables. The multi-annual average precipitation rates are in most cases reproduced or overestimated in complex regions. The distribution of daily precipitation intensity is in lesser agreement with GPCP and TRMM observation-based datasets, with simulated precipitation distribution often shifted from those observed towards higher or lower precipitation rates. The shapes of distributions are, however, usually well reproduced. The diurnal cycles of precipitation show the ability of the model to reproduce the afternoon increase in precipitation. The annual mean simulated climatology reveals weak cold bias and slightly overestimated precipitation for most subdomains.

The ability of the CRCM5 model to simulate the NAM has been assessed by comparing the precipitation patterns in two small subdomains, one in the core area of the NAM activity and another one in the northern limit of NAM area (AZNM). In the NAM core, the model reproduced correctly the precipitation annual cycle, including the NAM timing and intensity. The precipitation frequency distribution does not contradict the two observation-based reference datasets and the diurnal cycle is reproduced, although with a bias of afternoon maximum towards earlier hours. The model is also capable of reproducing the annual timing, daily precipitation frequency distribution and diurnal cycle (with a similar bias) of the NAM at its northern limit; however, CRCM5 underestimates by $\sim 30\text{--}40\%$ the strength of NAM in this area. The NAM being very sensitive to external factors, such as the SST both in coastal waters and in remote regions, it is difficult to estimate to which degree this imperfection is related to the model or to the external forcing.

The ability of the CRCM5 model to correctly simulate the GPLLJ has been assessed. The spatial and temporal structure of the meridional wind over the Great Plains has been studied in comparison with ERA-Interim reanalysis. It was shown that the model reproduces well the spatial extent and diurnal cycle of the GPLLJ, including the night-time wind intensity maximum. However, the characteristic night-time maximum of GPLLJ-related precipitation is only weakly reproduced by the model. It was shown that the area of night-time precipitation maximum is shifted

northwards from the GPLLJ zone in observations and this shift is well reproduced by the model.

The performance of CRCM5 has been largely improved in comparison with earlier versions of CRCM3 and CRCM4, especially in simulating precipitation, and it is comparable with that of other state-of-the-art RCMs under similar conditions.

In general, the performance of the CRCM5 model in reproducing the current climate of the North American continent in reanalysis-driven simulation can be considered as satisfactory and comparable to other state-of-the-art RCMs. The model has demonstrated a sound performance in reproducing complex precipitation patterns, which indicates its ability to adequately simulate underlying atmospheric phenomena and near-surface processes. While more work is required to understand and correct the imperfections revealed in this study, the CRCM5 performance in simulating the current climate forms a reliable basis for simulating the future climate within the CORDEX project framework.

Acknowledgments This work was supported by the Québec's *Ministère du Développement Économique, Innovation et Exportation* (MDEIE), the Canadian Foundation for Climate and Atmospheric Sciences (CFCAS), the Natural Sciences and Engineering Research Council of Canada (NSERC), Hydro-Québec, the Ouranos Consortium on Regional Climatology and Adaptation to Climate Change, the Mathematics of Information Technology and Complex Systems (MITACS) Network of Centres of Excellence, and the Canada Research Chairs programme. Some calculations were made on the high-performance computing platforms of the CLUMEQ Consortium, member of the Compute Canada and Calcul Québec. The authors thank Mr. Georges Huard and Mrs. Nadjet Labassi for maintaining an efficient and user-friendly local computing facility. The authors are also grateful to the following collaborators at Environment Canada: Mr. Michel Desgagné for his work in developing a nested version of GEM, Dr. Diana Versegny for allowing to use CLASS 3.5, Mr. Richard Harvey for CLASS-related discussions, and Mr. Ross Brown for discussions on observational database biases. This study would not have been possible without the access to valuable data from ERA40, ERA-Interim, CRU, UDEL, GPCP and TRMM.

Open Access This article is distributed under the terms of the Creative Commons Attribution License which permits any use, distribution, and reproduction in any medium, provided the original author(s) and the source are credited.

References

- Adler RF, Huffman GJ, Chang A, Ferraro R, Xie P, Janowiak J, Rudolf B, Schneider U, Curtis S, Bolvin D, Gruber A, Susskind J, Arkin P (2003) The version 2 global precipitation climatology project (GPCP-1dd) monthly precipitation analysis (1979-present). *J Hydrometeorol* 4:1147–1167
- Amador JA (1998) A climatic feature of the tropical Americas: the trade wind easterly jet. *Top Meteorol Oceanogr* 5(2):1–13
- Anderson CJ et al (2003) Hydrologic processes in regional climate model simulations of the central United States flood of June–July 1993. *J Hydrometeorol* 4:584–598

- Bélaïr S, Mailhot J, Girard C, Vaillancourt P (2005) Boundary layer and shallow cumulus clouds in a medium-range forecast of a large-scale weather system. *Mon Weather Rev* 133:1938–1960
- Benôit R, Côté J, Mailhot J (1989) Inclusion of a TKE boundary layer parameterization in the Canadian regional finite-element model. *Mon Weather Rev* 117:1726–1750
- Blackadar AK (1957) Boundary layer wind maxima and their significance for the growth of nocturnal inversions. *Bull Am Meteorol Soc* 38:283–290
- Brochu R, Laprise R (2007) Surface water and energy budgets over the Mississippi and Columbia river basins as simulated by two generations of the Canadian Regional Climate Model. *Atmos Ocean* 45:19–35
- Bukovsky MS (2011) Masks for the Bukovsky regionalization of North America. Regional Integrated Sciences Collective, Institute for Mathematics Applied to Geosciences, National Center for Atmospheric Research, Boulder, CO. [<http://www.narccap.ucar.edu/contrib/bukovsky/>]. Downloaded 05 July 2012
- Bukovsky MS, Karoly DJ (2011) A regional modeling study of climate change impacts on warm-season precipitation in the central United States. *J Clim* 24:1985–2002
- Castro CL, Pielke RA, Adegoke JO, Schubert SD, Pegion PJ (2007) Investigation of the summer climate of the contiguous United States and Mexico using the Regional Atmospheric Modeling System (RAMS). Part II: model climate variability. *J Clim* 20:3866–3887. doi:10.1175/JCLI4212.1
- Cerezo-Mota R, Allen M, Jones R (2011) Mechanisms controlling precipitation in the northern portion of the North American Monsoon. *J Clim* 24:2771–2783. doi:10.1175/2011JCLI3846.1
- Chakraborty A, Krishnamurti TN (2003) Numerical simulation of the North American monsoon system. *Meteorol Atmos Phys* 84:57–82. doi:10.1007/s00703-002-0566-6
- Collier JC, Zhang GJ (2006) Simulation of the North American monsoon by the NCAR CCM3 and its sensitivity to convection parameterization. *J Clim* 19:2851–2866
- Cook KH, Vity EK, Launer ZS, Patricola CM (2008) Springtime intensification of the Great Plains Low-Level Jet and Midwest precipitation in GCM simulations of the twenty-first century. *J Clim* 21:6321–6340. doi:10.1175/2008JCLI2355.1
- Cosgrove BA et al (2003) Real-time and retrospective forcing in the North American Land Data Assimilation System (NLDAS) project. *J Geophys Res* 108:8842. doi:10.1029/2002JD003118
- Côté J, Gravel S, Méthot A, Patoine A, Roch M, Staniforth A (1998) The operational CMC-MRB global environmental multiscale (GEM) model. Part I: design considerations and formulation. *Mon Weather Rev* 126:1373–1395
- de Elía R, Côté H (2010) Climate and climate change sensitivity to model configuration in the Canadian RCM over North America. *Meteorol Z* 19:325–339. doi:10.1127/0941-2948/2010/0469
- Dee DP et al (2011) The ERA-Interim reanalysis: configuration and performance of the data assimilation system. *Q J R Meteorol Soc* 137:553–597. doi:10.1002/qj.828
- Delage Y (1997) Parameterising sub-grid scale vertical transport in atmospheric models under statically stable conditions. *Bound Layer Meteorol* 82:23–48
- Delage Y, Girard C (1992) Stability functions correct at the free convection limit and consistent for both the surface and Ekman layers. *Bound Layer Meteorol* 58:19–31
- Giorgi F, Jones C, Asrar G (2009) Addressing climate information needs at the regional level: the CORDEX framework. *WMO Bull* 58:175–183
- Gutowski WJ, Takle ES, Arritt RW (1998) Project to intercompare regional climate simulations, Workshop II, 5–6 June 1997. *Bull Am Meteorol Soc* 79:657–659
- Gutowski WJ Jr, Arritt RW, Kawazoe S, Flory DM, Takle ES, Biner S, Caya D, Jones RJ, Laprise R, Leung LR, Mearns LO, Moufouma-Okia W, Nunes AMB, Qian Y, Roads JO, Sloan LC, Snyder MA (2010) Regional extreme monthly precipitation simulated by NARCCAP RCMs. *J Hydrometeorol* 11:1373–1379. doi:10.1175/2010JHM1297.1
- Gutzler DS et al (2005) The North American Monsoon Model Assessment Project: integrating numerical modeling into a field based process study. *Bull Am Meteorol Soc* 86:1423–1429
- Gutzler DS et al (2009) Simulations of the 2004 North American Monsoon: NAMAP2. *J Clim* 22:6716–6740. doi:10.1175/2009JCLI3138.1
- Hernández-Díaz L, Laprise R, Sushama L, Martynov A, Winger K, Dugas B (2012) Climate simulation over the CORDEX-Africa domain using the fifth-generation Canadian Regional Climate Model (CRCM5). *Clim Dyn*. doi:10.1007/s00382-012-1387-z
- Higgins RW, Gochis D (2007) Synthesis of results from the North American monsoon experiment (NAME) process study. *J Clim* 20:1601–1607. doi:10.1175/JCLI4081.1
- Higgins RW, Yao Y, Yarosh ES, Janowiak JE, Mo KC (1997) Influence of the Great Plains Low-Level Jet on summertime precipitation and moisture transport over the central United States. *J Clim* 10:481–507. doi:10.1175/1520-0442(1997)010<0481:IOTGPL>2.0.CO;2
- Holton JR (1967) The diurnal boundary layer wind oscillation above sloping terrain. *Tellus* 19:199–205
- Hu Q, Feng S (2002) Interannual rainfall variations in the North American summer monsoon region: 1900–98. *J Clim* 15:1189–1202. doi:10.1175/1520-0442(2002)015<1189:IRVITN>2.0.CO;2
- Huffman GJ, Adler RF, Morrissey M, Bolvin DT, Curtis S, Joyce R, McGavock B, Susskind J (2001) Global precipitation at one-degree daily resolution from multi-satellite observations. *J Hydrometeorol* 2:36–50
- Jiang X, Lau NC, Held IM, Ploshay JJ (2007) Mechanisms of the Great-Plains low-level jet as simulated in an AGCM. *J Atmos Sci* 64:532–547
- Jiao Y, Caya D (2006) An investigation of the summer precipitation simulated by the Canadian Regional Climate Model. *Mon Weather Rev* 134:919–932
- Kain JS, Fritsch JM (1990) A one-dimensional entraining/detraining plume model and application in convective parameterization. *J Atmos Sci* 47:2784–2802
- Kanamitsu M, Ebisuzaki W, Woollen J, Yang SK, Hnilo JJ, Fiorino M, Potter GL (2002) NCEP–DOE AMIP-II reanalysis (R-2). *B Am Meteorol Soc* 83:1631–1643
- Kourzeneva E (2010) External data for lake parameterization in numerical weather prediction and climate modeling. *Boreal Env Res* 15:165–177
- Kuo HL (1965) On formation and intensification of tropical cyclones through latent heat release by cumulus convection. *J Atmos Sci* 22:40–63
- Laprise R (1992) The Euler equation of motion with hydrostatic pressure as independent coordinate. *Mon Weather Rev* 120:197–207
- Laprise R, Hernández-Díaz L, Tete K, Sushama L, Šeparović L, Martynov A, Winger K, Valin M (2013) Climate projections over CORDEX Africa domain using the fifth-generation Canadian Regional Climate Model (CRCM5). *Clim Dyn*. doi:10.1007/s00382-012-1651-2
- Lee MI et al (2007) An analysis of the warm-season diurnal cycle over the continental United States and northern Mexico in general circulation models. *J Hydrometeorol* 8:344–366. doi:10.1175/JHM581.1
- Li J, Barker HW (2005) A radiation algorithm with correlated-k distribution. Part I: local thermal equilibrium. *J Atmos Sci* 62:286–309

- Lin J-L, Mapes EB, Weickmann KM, Kiladis GN, Schubert SD, Suarez MJ, Bacmeister JT, Lee M-I (2008) North American Monsoon and convectively coupled equatorial waves simulated by IPCC AR4 coupled GCMs. *J Clim* 21:2919–2937. doi:[10.1175/2007JCLI1815.1](https://doi.org/10.1175/2007JCLI1815.1)
- Martynov A, Sushama L, Laprise R, Winger K, Dugas B (2012) Interactive lakes in the Canadian Regional Climate Model, version 5: the role of lakes in the regional climate of North America. *Tellus A* 64:16226. doi:[10.3402/tellusa.v64i0.16226](https://doi.org/10.3402/tellusa.v64i0.16226)
- Masson V, Champeaux J-L, Chauvin F, Meriguet Ch, Lacaze R (2003) A global database of land surface parameters at 1-km resolution in meteorological and climate models. *J Clim* 16:1261–1282. doi:[10.1175/1520-0442-16.9.1261](https://doi.org/10.1175/1520-0442-16.9.1261)
- McFarlane NA (1987) The effect of orographically excited gravity-wave drag on the circulation of the lower stratosphere and troposphere. *J Atmos Sci* 44:1175–1800
- McPhee J, Margulis SA (2005) Validation and error characterization of the GPCP-1DD precipitation product over the contiguous United States. *J Hydrometeorol* 6:441–459. doi:[10.1175/JHM429.1](https://doi.org/10.1175/JHM429.1)
- Mearns LO (2010) The North American regional climate change assessment program: an overview Kansas NSF EPSCor conference, University of Kansas, Lawrence, Kansas October 4, 2010. http://www.nsfepscor.ku.edu/pdf/20101004_Mearns.pdf. Accessed 12 Feb 2011
- Mearns LO, Gutowski WJ, Jones R, Leung L-Y, McGinnis S, Nunes AMB, Qian Y (2009) A regional climate change assessment program for North America. *EOS* 90:11–312
- Mearns LO et al (2012) The North American regional climate change assessment program: overview of phase 1 results. *Bull Am Meteorol Soc* 93:1337–1362. doi:[10.1175/BAMS-D-11-00223.1](https://doi.org/10.1175/BAMS-D-11-00223.1)
- Mironov D, Heise E, Kourzeneva E, Ritter B, Schneider N, Terzhevik A (2010) Implementation of the lake parameterisation scheme FLake into the numerical weather prediction model COSMO. *Boreal Environ Res* 15:218–230
- Mitchell TD, Jones PD (2005) An improved method of constructing a database of monthly climate observations and associated high-resolution grids. *Int J Climatol* 25:693–712. doi:[10.1002/joc.1181](https://doi.org/10.1002/joc.1181)
- Mitchell DL, Ivanova D, Rabin R, Brown TJ, Redmond K (2002) Gulf of California sea surface temperatures and the North American Monsoon: mechanistic implications from observations. *J Clim* 15:2261–2281. doi:[10.1175/1520-0442\(2002\)015<2261:GOCSSST>2.0.CO;2](https://doi.org/10.1175/1520-0442(2002)015<2261:GOCSSST>2.0.CO;2)
- Mladjic B, Sushama L, Khaliq MN, Laprise R, Caya D, Roy R (2011) Canadian RCM projected changes to extreme precipitation characteristics over Canada. *J Clim* 24:2565–2584. doi:[10.1175/2010JCLI3937.1](https://doi.org/10.1175/2010JCLI3937.1)
- Mo KC, Chelliah M, Carrera ML, Higgins RW, Ebisuzaki W (2005) Atmospheric moisture transport over the United States and Mexico as evaluated in the NCEP regional reanalysis. *J Hydrometeorol* 6:710–728. doi:[10.1175/JHM452.1](https://doi.org/10.1175/JHM452.1)
- Music B, Caya D (2007) Evaluation of the hydrological cycle over the Mississippi river basin as simulated by the Canadian Regional Climate Model (CRCM). *J Hydrometeorol* 8:969–988. doi:[10.1175/JHM627.1](https://doi.org/10.1175/JHM627.1)
- Paquin D, Laprise R, Winger K, de Elía R, Zadra A, Dugas B (2009) Climate simulations over North America with the Canadian Regional Climate Model (CRCM): from operational version 4 to developmental version 5. “21st Century Challenges in Regional-scale Climate Modelling”, 2nd International Lund RCM Conference, 4–8 May 2009, Lund (Sweden), pp 109–110. http://www.baltex-research.eu/RCM2009/Material/RCM2009_Proceedings_print.pdf. Accessed 26 July 2012
- Plummer DA, Caya D, Frigon A, Côté H, Giguère M, Paquin D, Biner S, Harvey R, de Elía R (2006) Climate and climate change over North America as simulated by the Canadian RCM. *J Clim* 19:3112–3132
- Rife DL, Pinto JO, Monaghan AJ, Davis CA, Hannan JR (2010) Global distribution and characteristics of diurnally varying low-level jets. *J Clim* 23:5041–5064
- Saleeby SM, Cotton WR (2004) Simulations of the North American monsoon system. Part I: model analysis of the 1993 monsoon season. *J Clim* 17:1997–2018
- Šeparović L, Alexandru A, Laprise R, Martynov A, Sushama L, Winger K, Valin M (2013) Present climate and climate change over North America as simulated by the fifth-generation Canadian Regional Climate Model (CRCM5). *Clim Dyn* (accepted)
- Stensrud DJ (1996) Importance of low-level jets to climate: a review. *J Clim* 9:1698–1711. doi:[10.1175/1520-0442\(1996\)009<1698:IOLLJT>2.0.CO;2](https://doi.org/10.1175/1520-0442(1996)009<1698:IOLLJT>2.0.CO;2)
- Stensrud DJ, Gall RL, Mullen SL, Howard KW (1995) Model climatology of the Mexican Monsoon. *J Clim* 8:1775–1794
- Sturm M, Holmgren J, König M, Morris K (1997) The thermal conductivity of seasonal snow. *J Glaciol* 43:26–41
- Sundqvist H, Berge E, Kristjansson JE (1989) Condensation and cloud parameterization studies with a mesoscale numerical weather prediction model. *Mon Weather Rev* 117:1641–1657
- Takele ES et al (1999) Project to intercompare regional climate simulations (PIRCS): description and initial results. *J Geophys Res* 104:19433–19461
- Tian B, Held IM, Lau N-C, Soden BJ (2005) Diurnal cycle of summertime deep convection over North America: a satellite perspective. *J Geophys Res* 110:D08108. doi:[10.1029/2004JD005275](https://doi.org/10.1029/2004JD005275)
- Uppala SM et al (2005) The ERA-40 re-analysis. *Q J R Meteorol Soc* 131:2961–3012. doi:[10.1256/qj.04.176](https://doi.org/10.1256/qj.04.176)
- Verseghy DL (1991) CLASS—a Canadian land surface scheme for GCMs: I. Soil model. *Int J Climatol* 11:111–133
- Verseghy DL (2009) CLASS—The Canadian Land Surface Scheme (Version 3.4)—technical documentation (version 1.1). Internal report, Climate Research Division, Science and Technology Branch, Environment Canada, p 183
- Wang S-Y, Chen T-C, Takele ES (2010) Climatology of summer midtropospheric perturbations in the U.S. Northern Plains. Part II: large-scale effects of terrain boundary layer on genesis. *Clim Dyn*. doi:[10.1007/s00382-010-0765-7](https://doi.org/10.1007/s00382-010-0765-7)
- Willmott CJ, Matsuura K (1995) Smart interpolation of annually averaged air temperature in the United States. *J App Meteorol* 34:2577–2586
- Yang D, Kane D, Zhang Z, Legates D, Goodison B (2005) Bias-corrections of long-term (1973–2004) daily precipitation data over the northern regions. *Geophys Res Lett* 32:L19501. doi:[10.1029/2005GL024057](https://doi.org/10.1029/2005GL024057)
- Yeh K-S, Côté J, Gravel S, Méthot A, Patoine A, Roch M, Staniforth A (2002) The CMC-MRB global environmental multiscale (GEM) model. Part III: nonhydrostatic formulation. *Mon Weather Rev* 130:339–356
- Zadra A, Roch M, Laroche S, Charron M (2003) The subgrid scale orographic blocking parametrization of the GEM model. *Atmos-Ocean* 41(2):155–170
- Zadra A, Caya D, Côté J, Dugas B, Jones C, Laprise R, Winger K, Caron L-P (2008) The next Canadian regional climate model. *Phys Can* 64:74–83
- Zadra A, McTaggart-Cowan R, Roch M (2012) Recent changes to the orographic blocking. Seminar presentation, RPN, Dorval, Canada, 30 March 2012. http://collaboration.cmc.ec.gc.ca/science/rpn/SEM/dossiers/2012/seminaires/2012-03-30/Seminar_2012-03-30_Ayrton-Zadra.pdf. Accessed 19 July 2012